
This manuscript is a **preprint** and has been submitted for publication in the **Journal of the Geological Society of London**. This version of the manuscript has been accepted for publication following peer review-review but has not undergone copyediting/typetting. Please feel free to contact any of the authors directly to comment on the manuscript.

July 19th 2022

1 Rivers of the Variscan Foreland: fluvial morphodynamics in the Pennant 2 Formation of South Wales, UK

3 James Wood¹, Jonah S. McLeod¹, Sinéad J. Lyster¹ and Alexander C. Whittaker^{1*}

4 ¹Department of Earth Science and Engineering, Imperial College London, UK, SW7 2BX.

5 *Correspondence (a.whittaker@imperial.ac.uk)

6 *note the above email will expire after July 2022 – alternatives include: a.whittaker@imperial.ac.uk,
7 s.lyster17@imperial.ac.uk & jonah.mcleod18@imperial.ac.uk*

8 Present address: (AW) 3.51, Royal School of Mines, South Kensington Campus, Prince Consort Road,
9 London SW7 2AZ

10 Abbreviated title: Rivers of the Variscan Foreland

11 ORCID: JW – 0000-0002-1673-0097, JM – 0000-0002-5382-3559, SL - 0000-0002-1188-533X, AW -
12 0000-0002-8781-7771.

13 Abstract

14 The morphodynamics of ancient rivers can be reconstructed from fluvial stratigraphy using
15 quantitative techniques to provide insights into the driving forces behind the sedimentary systems.
16 This work explores how these drivers can be evaluated from Paleozoic stratigraphy. Field
17 measurements are taken in fluvial sediments from the Westphalian (Bolsovian and Asturian; 315.2–
18 308 Ma) Pennant Formation of South Wales, UK, to reconstruct the hydrodynamics and morphologies
19 of these Carboniferous rivers, which were sourced from the Variscan (Hercynian) Mountain belt
20 located south of the study area. Field data consist of cross-set heights, grain size, palaeocurrent
21 directions, and the dimensions of fluvial architectural elements. Hydrodynamic properties, including
22 flow velocities and discharge rates, are reconstructed using a suite of numerical approaches. Results
23 suggest median formative flow depths of 2–3 m and palaeoslopes of $4\text{--}5 \times 10^{-4}$ (0.02–0.03°).
24 Quantitative planform prediction suggests these rivers were likely anastomosing but with distinct
25 single-threaded reaches. Mean single-thread width is 55 m, while mean channel-belt widths of 100–
26 200 m are reconstructed, suggesting bankfull discharges of 390–560 m³ s⁻¹. This study resolves
27 contrasting palaeohydrological interpretations for Pennant rivers, and demonstrates how
28 reconstructions of morphology, slope and planform can be obtained from fluvial stratigraphy.

29

30

31 **Supplementary Material**

32 Field data, a field localities KMZ file, analysis of flow depth scaling methods, and fluvial facies analysis
33 is available at xxxxxxxx.

34

35

36

37

38 Rivers have been among the most significant drivers of geomorphological and hydrological change on
39 Earth's surface since the Archean (Hjellbakk 1997; Eriksson et al. 2006; Gibling & Davies 2012; Ielpi et
40 al. 2017; Bridgland et al. 2014, Ganti et al. 2019). Their hydrodynamic and morphodynamic properties
41 are recorded in the stratigraphic record (Whittaker 2012; Ganti et al. 2014, Bhattacharya et al. 2016),
42 allowing researchers to reconstruct the characteristics and behaviour of ancient fluvial systems from
43 the geological archive (e.g., Michael et al. 2014; Ganti et al. 2019; Chamberlin & Hajek 2019; Lyster et
44 al. 2021). These reconstructions include morphologic and hydrodynamic properties (Paola & Mohrig
45 1996; Duller et al. 2012; Chen et al. 2018; Shibata et al. 2018; Greenberg & Hajek 2021), sediment
46 transport capacity (Holbrook and Wanas 2014; Li & Bhattacharya 2017; Sharma et al. 2017; Mahon
47 and McElroy 2018), and drainage area and shape (Bhattacharya and Tye 2004; Bhattacharya et al.
48 2016; Xu et al. 2017; Li et al. 2018; Lyster et al., 2020). As river development is closely linked to tectonic
49 and climatic forcing, fluvial strata provide insights into the prevailing tectono-climatic conditions at
50 the time of deposition (Duller et al. 2010; Castelltort et al. 2012; Whittaker 2012; Harries et al. 2021).

51 While much work in the field of sedimentology has implemented qualitative techniques (e.g., facies
52 analysis) to provide valuable insights into river characteristics from fluvial strata (e.g., Jones 1977;
53 Miall 1985; Bridge 2003; Plink-Bjorklund 2015, amongst many others), an increasing number of
54 quantitative approaches are beginning to present new opportunities within the discipline. Empirical
55 and theoretical equations can be used to reconstruct the morphology and hydrology of modern rivers
56 in terms of slope, depth, and water discharge (Leopold and Maddock Jr. 1953; Hack 1957; Leopold and
57 Wolman 1960; Williams 1984). These methods have been increasingly adapted for stratigraphic
58 application in recent years to facilitate multifaceted reconstructions of ancient systems (Bridge and
59 Mackey 1992; Leclair and Bridge 2001; Trampush et al. 2014; Bradley and Venditti 2017; Greenberg
60 et al. 2021; Lyster et al., 2022), enabling fluvial morphodynamics such as channel dimensions, flow
61 velocities and unit discharges to be quantified in a way that is not possible from qualitative facies
62 analyses alone. Reconstruction of river behaviour within this type of palaeohydrological framework

63 therefore adds richness to insights offered from more classical sedimentological approaches, and in
64 some cases may even challenge pre-existing interpretations (e.g. Ganti et al, 2019). However, utilising
65 quantitative palaeohydrological techniques can be restricted by the incomplete nature of the rock
66 record (Sadler 1981; Straub et al. 2020). Additionally, the limited number of data sets to-date of
67 ancient river deposits where important sedimentological observables (e.g., height and distributions of
68 cross-beds) are quantified with sufficient precision means robust reconstructions of fluvial
69 morphodynamics are rare (c.f. Leary & Ganti 2019; Lyster et al. 2022). Nonetheless, in principle,
70 palaeohydrological studies offer an opportunity to assess the scale and dimensions of ancient fluvial
71 landscapes, particularly where the corresponding geomorphic archive has been lost, and to quantify
72 the fluxes of sediment and water across the surface of the Earth and other planets in the geological
73 past (Ganti et al. 2019; Stack et al. 2019; Lyster et al. 2021).

74 This study focuses on the palaeohydrology of Upper Carboniferous (Pennsylvanian) fluvial systems of
75 the Pennant Sandstone Formation, South Wales, UK (Figure 1). In the UK, the Upper Carboniferous
76 comprises the Namurian, Westphalian, Stephanian and Autunian regional stages, with the
77 Westphalian stage, which is the subject of this study, spanning 319 Ma to 308 Ma (Davydov et al.
78 2012). Further, the Westphalian stage comprises the Langsettian, Duckmantian, Bolsovian and
79 Asturian regional substages, with the Bolsovian and Asturian substages being the focus here
80 (315.2–308 Ma; Davydov et al. 2012).

81 The Pennant Sandstone is of key interest due to its tectono-geographic setting in the foreland of the
82 Variscan Orogen, temporally close to the cessation of the northward migration of the Variscan front
83 during the Westphalian stage (Gayer and Jones 1989; Jones 1991; Burgess and Gayer 2000; Opluštil
84 and Cleal 2007). Hence, these strata record the behaviour, water discharges, and sediment fluxes of
85 rivers during the latter stages of the assembly of the Pangaeon supercontinent. The formation crops
86 out extensively in the South Wales and Pembrokeshire Coalfields and has a well-constrained
87 stratigraphic framework owing to geological studies during Wales' time as a productive coal mining
88 region (Woodland et al. 1957; Kelling 1974; Jones 1977). Previous sedimentological work on the
89 Pennant has largely centred on qualitative facies and architectural observations to build a nuanced
90 picture of river behaviour and environment in the upper Carboniferous (De la Beche 1846, Strahan
91 1899, Woodland et al. 1957, Kelling 1974, Jones 1977; Jones & Hartley, 1993). These classic studies
92 provide detailed sedimentological context for our work. However to date, the morphodynamic and
93 hydrodynamic characteristics of these fluvial systems have not been reconstructed using a
94 quantitative palaeohydrological framework. Here we revisit the Pennant Formation and use
95 palaeohydrological approaches, founded in bedform analysis (c.f. Ganti et al. 2019; Lyster et al. 2021),
96 to exemplify how new insights into fluvial system behaviour can be obtained for classic geological

97 formations that have received little recent study. Consequently, our field data allow us to reconstruct
98 flow depths, palaeoslopes, water discharges, and the behaviour of Carboniferous rivers draining the
99 northern margin of the Variscan mountain belt. These results provide insight into how ancient fluvial
100 systems responded to foreland basin evolution during a major orogenic event and demonstrate how
101 channel planform and characteristics can now be extracted from quantitative measurements of fluvial
102 stratigraphy.

103 **Regional Tectono-stratigraphy**

104 The Pennant Sandstone Formation comprises Bolsovian and Asturian aged fluvial sediments that were
105 deposited in the South Wales foreland basin (Figure 1a) by rivers draining mountainous terrain built
106 during the Variscan orogeny (Kelling 1974; Evans 2004). Today, these sediments crop out in the South
107 Wales and Pembrokeshire Coalfields. The Variscan (Hercynian) Orogeny was the principal formative
108 orogenic event of the supercontinent Pangaea, creating an orogenic belt that stretched east–west
109 over 1000 km (Leveridge and Hartley 2006). Many of the north–south orientated compressional
110 structures and sedimentary basins of Europe today can be attributed to the Variscan Orogeny,
111 including the South Wales and Pembrokeshire coalfields that form the geographical focus of this study
112 (Leveridge and Hartley 2006, Opluštil and Cleal 2007). The South Wales foreland basin, situated to the
113 north of the northward propagating Variscan Orogenic Belt (Figure 1c), was generated following
114 inversion of a regional Devonian–Lower Carboniferous extensional regime (Hartley and Warr 1990;
115 Burgess and Gayer 2000; Opluštil and Cleal 2007). The northern edge of the foreland was bounded by
116 the cratonic upland of the Wales-Brabant High (Figure 1c; Rippon 1996).

117 By the end of the Carboniferous, the front of Variscan deformation had migrated northward to the
118 location of the South Wales Coalfield, producing shortening of up to 30% and north–south
119 compressional structures such as the major asymmetric syncline that dominates the structure of the
120 coalfield today (Figure 1b; Jones 1991; Gayer and Pesek 1992; Evans 2004). Subsidence curves of the
121 South Wales Basin suggest a rapid accommodation generation of 260 m Myr⁻¹ in the west and 130 m
122 Myr⁻¹ in the east during the late Westphalian (Burgess and Gayer 2000). As the underlying South Wales
123 Coal Measures consist of sediment sourced from the Wales-Brabant High (Evans 2004), the base of
124 the Pennant Formation represents the onset of Variscan deposition in the region (Leveridge and
125 Hartley 2006; Opluštil and Cleal 2007).

126 The Pennant sandstone has a maximum total thickness of 1350 m and is subdivided into 5 members
127 shown in Figure 2 (Barclay 2011). These members, first described as ‘beds’ by Woodland et al. (1957)
128 following the early classification work of De La Beche (1846) and Strahan (1899), are separated by coal
129 horizons and form the basis for temporal differentiation in this study. Each member contains

130 sandstone (greenish-grey, lithic arenite), mudstone, siltstone, and coals of varying abundances and
131 thicknesses (Waters et al. 2007; Waters et al. 2009). The Rhondda Member is the thickest and contains
132 the highest proportion of sand (Waters et al. 2009) so is, therefore, the most represented member in
133 outcrop. The Llynfi, Hughes, and Swansea members have limited outcrop due to higher proportion of
134 muds and silts, while the Brithdir Member's lesser thickness also limits the abundance of outcrop
135 (Waters et al. 2009). While the exact stratigraphic boundary between the Bolsovian and Asturian
136 substages is not formally defined in the Pennant Sandstone, it is considered to be within the Brithdir
137 Member's depositional timespan (Waters et al. 2009; Barclay 2011).

138 The base of the Pennant Formation is described as the first significant 'Pennant-type' sandstone
139 (greenish-grey and blueish-grey, feldspathic, micaceous, lithic arenite) of at least 3 m thickness
140 (Waters et al. 2009), creating a diachronicity of the horizon. In the Swansea region, the base is
141 contemporaneous with the Cambriense Marine Band at the base of the Llynfi Member (Barclay 2011)
142 whilst the base rises as high in the stratigraphy as the Brithdir Member in the eastern coalfield (Waters
143 et al. 2009). The top of the Pennant Sandstone is also diachronous with the Swansea Member absent
144 in the east of the coalfield (Waters et al. 2009). The diachronous boundary means the variability of
145 thickness of the Pennant is high (Figure 2), particularly across the Neath Disturbance, a major
146 northeast–southwest trending Caledonoid fault in the modern Vale of Neath (Barclay 2011).

147 Correlation of the Pennant Sandstone between the Pembrokeshire and South Wales Coalfields is
148 contentious with an early study suggesting correlation of Pembrokeshire outcrops with the Hughes
149 Member (Jenkins 1962). More recently, a palaeobotanical study conducted by Cleal and Thomas
150 (1992) correlated these deposits with the Rhondda Member. Herein, the Pembrokeshire Pennant is
151 included in the Rhondda Member.

152 Although there has been little recent work on the sedimentology of the Pennant Formation, previous
153 studies in the last 50 years have generally described the depositional environment of the Pennant
154 Sandstone as a low-sinuosity, relatively proximal braidplain, characterised by development of sheet-
155 like or stacked sandstone bodies, a concentration of in-channel bedforms and a general absence of
156 point bar deposits (Kelling 1969; Jones 1977; Jones and Hartley 1993). The doctoral thesis of Jones
157 (1977), for instance, includes extensive and detailed analyses of architectural features and facies
158 within the lower Pennant, and our study makes use of this significant body of work. Jones in particular
159 identifies two major facies associations; the first is interpreted as the result of repeated incursions of
160 small deltas, or crevasse deltas, into shallow bays, and the second, which is dominant after the Llynfi
161 member, is interpreted to record braided rivers characterised by a variable discharge regime, which
162 laterally migrated through a vegetated floodplain environment. Although Jones (1977) rejects the

163 notion of the Pennant recording classical meandering channels (*sensu* Allen 1963) and estimates
164 channel widths of order hundreds of metres, their thesis also suggests that individual channels may
165 have had flow depths of >15 m based on channel body thicknesses, which would have been unusually
166 deep for braided systems. This example serves to underscore the potential discrepancies between
167 facies-derived reconstructions presented in the historic literature and morphodynamic
168 considerations. Consequently, our work allows for a re-evaluation of the characteristics of these
169 Carboniferous fluvial systems that drained the growing Variscan orogen for the 21st Century.

170 **Study Methods**

171 **Field Data Collection**

172 Field data were collected in the South Wales Coalfield (17 localities) and Pembrokeshire Coalfield (2
173 localities) during two field campaigns in August and September 2021. All measurements were taken
174 in channelized sandstone bodies and form the basis of the reconstruction and analysis of river
175 morphologies in this study.

176 *Cross-sets*

177 Cross-sets in medium to very-coarse sands were measured to reconstruct the sizes of bedforms in
178 Pennant rivers using the method of Leclair and Bridge (2001). This approach requires mean cross-set
179 heights, so distributions of heights in individual cross-sets ($n = 268$) were measured to the nearest 10
180 mm at 10 cm intervals along the major axis of the cross-set (7 to 62 measurements per cross-set;
181 Figure 3b). From these height distributions, mean cross-set heights, h_{xs} , were subsequently extracted.
182 Maximum heights were also extracted from the distributions to derive a scaling factor between mean–
183 maximum cross-set heights for each member of the Pennant Sandstone. This method has successfully
184 been used previously on fluvial strata in Utah, USA (Lyster et al. 2021), and northwest Scotland (Ganti
185 et al. 2019).

186 Cross-set height maxima were also measured at each locality ($n = 1809$; Figure 3d). Using the new
187 mean–maximum height scaling factors, mean cross-heights were estimated for each measured
188 maximum height, expanding the total dataset from 268 to 2077 mean cross-set heights.

189 Palaeocurrent directions were determined at each field site by measuring the dip and dip direction of
190 cross-set lee slopes ($n = 1038$). Bedding measurements were also taken at each site or from geological
191 maps ($n = 58$). Palaeocurrent measurements were subsequently unfolded using *Stereonet 11*
192 (Allmendinger 2020) to correct for the dip of beds and therefore decipher true palaeocurrent
193 directions of the rivers recorded within each member of the Pennant Formation.

194 *Grain size*

195 Where the height distribution of an individual cross-set was measured, the median grain size, D_{50} , was
196 also estimated using the Wentworth grainsize classification (Wentworth 1922; Figure 3e) and
197 converted to a numerical value in metres (e.g., 0.000375 m for medium sand, 0.0005 m for
198 medium-coarse sand etc.). Grain-size photographs were also taken at each locality to later verify the
199 estimated grainsize using *ImageJ* software (Rasband 2018). Grain-sizes exceeding sand grade were
200 observed in some outcrops of the Pennant Sandstone, and typically occurred as isolated lenses at the
201 base of channel fills (Figure 3f; c.f. Jones 1977; Jones & Hartley 1993). Distributions of these
202 conglomeratic sediments were measured using the Wolman point count method (Wolman 1954) to
203 extract D_{50} and were used to constrain the maximum possible, but rare, flow conditions in Pennant
204 rivers.

205 *Architectural fluvial elements*

206 To validate the palaeohydrological reconstructions, the dimensions of bar-scale (1-10s m scale)
207 architectural elements were independently measured (Figure 4). The heights of both channel fill
208 sandstone packages and accretion packages (downstream and lateral) were quantified using a laser
209 range finder (Haglöf Laser Geo) to a precision of 0.1 m ($n = 116$). These accretion packages,
210 representing bar-scale clinoforms, provide a maximum bankfull flow depth where the total height of
211 the bar-clinoform is visible, or where it can be extrapolated (Mohrig et al. 2000; Hajek and Heller
212 2012). These estimates of bankfull flow depth were used to validate flow depths calculated from cross-
213 set heights. Where possible, accretion package widths were measured for channel width calculations
214 (below) and outcrop-scale photographs were taken to show the fluvial architecture of each site (Figure
215 4).

216 **Palaeohydrology**

217 *Flow depth*

218 Cross-set heights represent a fraction of the original bedform height. Here, the scaling relation of
219 Leclair and Bridge (2001) was used to convert mean cross-set height, h_{xs} , to mean bedform height, h_d :

220
$$h_d = 2.9(\pm 0.7)h_{xs} \quad (1)$$

221 This relationship is based on the theoretical model of Paola and Borgman (1991) for bedform
222 migration over random topography on the bed with negligible angle of climb. Here, uncertainty of the
223 scaling factor (± 0.7) represents the standard deviation of the dataset used by Leclair and Bridge (2001).
224 To account for this uncertainty, a Monte Carlo uncertainty propagation method was used, following

225 the method of Lyster et al. (2021). 10^6 random values of the model parameter were generated
226 between the uncertainty intervals ($2.9 + 0.7$ and $2.9 - 0.7$ for Eq. 1) and were used to calculate h_d . This
227 recovered 10^6 values of h_d which were subsequently carried forwards — Monte Carlo uncertainty
228 propagation was used in all subsequent equations presented here with the stated uncertainties, and
229 the outcome of these calculations, below, are presented as box and whisker plots which show the
230 median and interquartile ranges for our palaeohydrological reconstructions in the results.

231 To estimate flow depth, H, the relationship of Bradley and Venditti (2017) was used:

$$232 \quad H = 6.7h_d \quad (2)$$

233 This relationship was derived following a reevaluation of past work on dune–depth scaling relations
234 that were deemed to be ineffective (Yalin 1964; van Rijn 1984; Julien and Klaassen 1995). The scaling
235 factor in Eq. 2 (i.e., 6.7) at 50% uncertainty has a range of 4.4–10.1. A Monte Carlo propagation was
236 again used between these values to accommodate this uncertainty. Any calculated values of H that
237 exceeded 125% of the maximum measured package thickness at the field site were removed from the
238 dataset at this stage (n = 89 out of more than 2000 cross-sets).

239 *Palaeoslope*

240 Slope, S, was reconstructed using estimates of D_{50} and H, and using the empirical method of Trampus
241 et al. (2014), which is appropriate for the range of grain sizes used in this study. Here Slope, S, is given
242 by:

$$243 \quad \log S = \alpha_0 + \alpha_1 \log D_{50} + \alpha_2 \log H \quad (3)$$

244 where α_0 , α_1 and α_2 are constants given as -2.08 ± 0.036 , 0.254 ± 0.016 , and -1.09 ± 0.044 respectively.
245 Monte Carlo uncertainty propagation was used to accommodate uncertainty in the constants
246 (Trampus et al. 2014). Palaeoslope values were analysed both temporally (i.e., between members)
247 and spatially (i.e., downstream considering resolved palaeocurrent directions where we have multiple
248 channel measurements at a similar stratigraphic level of the Pennant).

249 *Flow velocity and unit discharge*

250 The equation of Manning et al. (1890) was used to derive flow velocity, U, and water discharge per
251 unit width, Q_U , as $Q_U = U \times H$. Manning's equation is given as:

$$252 \quad U = \frac{1}{n} H^{\frac{2}{3}} S^{\frac{1}{2}} \quad (4)$$

253 where n, Manning's Roughness Coefficient, is approximated as 0.03 following Lyster et al. (2021)
254 based on the value for fluvial channels of the look-up table of Chow (1959). U is given in m s^{-1} and Q_U

255 is given in $\text{m}^2 \text{s}^{-1}$. Q_U can be multiplied by an estimated width, W , to give total bankfull discharge, Q ,
256 in $\text{m}^3 \text{s}^{-1}$.

257 *Fluvial style and channel widths*

258 Determining the planform morphology of ancient river systems can be difficult as preservation of
259 entire channels is rare in the rock record (Brierley 1989; Parker 1976; Lyster et al. 2022). Traditionally,
260 facies analyses of architectural elements using vertical profiles and plan-view exposures of fluvial
261 strata are used to classify ancient rivers as meandering, straight, anastomosing, or braided (Miall
262 1985). However, these analyses are most effective where outcrop is complete. Therefore, quantitative
263 techniques using the Froude number (Fr), S , and aspect ratio (i.e., the ratio of channel width, W , to
264 channel depth, H) of channels can also be implemented to determine fluvial style. Fr is calculated
265 using:

$$266 \quad Fr = \frac{U}{\sqrt{gH}} \quad (5)$$

267 where g is gravitational acceleration.

268 Stability fields for braided and meandering channels can be reconstructed using plots of S/Fr against
269 the inverse of channel aspect ratio (i.e., H/W as opposed to W/H), as the seminal work of Parker (1976)
270 originally showed. Recently, Lyster et al. (2022) re-evaluated the stability fields of Parker (1976) using
271 a new dataset of nearly 1700 modern rivers. They showed that $H/W < 0.02$ characterises multi-thread
272 systems and $H/W > 0.02$ characterises single-thread systems, while $S/Fr > 0.003$ characterises braided
273 multi-thread systems and $S/Fr < 0.003$ characterises anastomosing multi-thread systems. Here, these
274 new insights were used to reconstruct channel planform for all members of the Pennant Formation.

275 The method of Greenberg et al. (2021) was used to quantify single-thread channel widths, W_C , where
276 lateral accretion package widths, W_L , were observed at field sites ($n = 23$).

$$277 \quad W_C = 2.34(\pm 0.13)W_L \quad (6)$$

278 Where lateral accretion packages were partially preserved, W_L was estimated by extrapolating
279 accretion surfaces using structural measurements of accretion surfaces relative to bedding. Monte
280 Carlo uncertainty propagation was used with the bounds of the scalar in Eq. 6. Across the mapped
281 extent of the Pennant, steeper-sided escarpments are generally composed of channel sandstones
282 whereas rolling grass-covered slopes are typically underlain by overbank fines of the Pennant.
283 Therefore, the width of sandstone outcrops provides a constraint on the maximum width of the
284 channel belt and, as such, were measured as an estimate of channel belt width, W (c.f. Jones, 1977).

285 In addition, a channel aspect ratio described in the thesis of Jones of 1:56, based on observations in
286 the Pennant at Rhondda Fawr, was also used to estimate W from reconstructed values of H .

287 **Results**

288 **Palaeohydrology**

289 Distributions of height within individual cross-sets demonstrate a linear relationship between mean
290 and maximum cross-set height (h_{xs} and h_{xsMax}), where h_{xs} is ~62% of the maximum cross-set height
291 (Figure 5a). Separating these data by member resulted in similar scaling relations in the range $h_{xs} =$
292 $0.59h_{xsMax}$ to $h_{xs} = 0.65h_{xsMax}$ (Figure 5b). These scaling relationships are comparable to those reported
293 by Lyster et al. (2021) for Upper Cretaceous fluvial strata in Utah, suggesting that mean cross-set
294 heights scale predictably with cross-set maxima. Using these member-specific scaling relationships, n
295 = 1809 cross-set height maxima were converted to mean cross-set heights, and these were used to
296 supplement the $n = 268$ mean cross-set heights from measured distributions. Of these $n = 2077$ mean
297 cross-set heights, the mean value is 0.12 m.

298 Mean cross-set heights correspond to median flow depths, H , in the Pennant Sandstone of 2.3 m using
299 Eq. 1 and 2, while taking channel/accretion packages heights as a proxy for H gives a median of 2.45
300 m (Fig. 6a). This suggests that results are robust with only 4% of calculated flow depths exceeding
301 125% of the maximum measured package height at the corresponding locality (Supplement 3). Figure
302 6 further summarises the hydrodynamic properties (H , S , U , and Q_U) reconstructed for the Pennant
303 Formation and its constituent members. As each measured cross-set has been used within our Monte
304 Carlo uncertainty propagation approach, the median and interquartile ranges of reconstructed fluvial
305 morphodynamics of Pennant rivers can be extracted and shown as box and whisker plots, grouped by
306 member. This grouping aims to maximise the potential to isolate any temporal trends in the data.
307 Flow depths reconstructed for all members are similar to the mean for the Pennant Sandstone as a
308 whole (2.3 m), with interquartile depth ranges of ca. 2 to 3 m. Only the Llynfi has marginally more
309 shallow channels than the succeeding members, but its interquartile range shows significant overlap
310 with the overlying succession (Fig. 6a). Palaeoslopes show limited temporal variation with all members
311 returning median slopes of 4.5×10^{-4} and interquartile ranges of ca. $4 - 6 \times 10^{-4}$ (my/mx; $0.02-0.03^\circ$),
312 values that are consistent with sand-bedded lowland rivers today (Fig. 6b; Trampush et al., 2014). No
313 statistically significant up-section change in S was observed following Kolmogorov-Smirnov tests
314 between each member (Supplement 5). Values of U and Q_U similarly show limited temporal variation
315 with median values ranging between $1.2-1.3 \text{ m s}^{-1}$ and $2-3 \text{ m}^2 \text{ s}^{-1}$ respectively, and interquartile
316 ranges which also overlap (Fig. 6c, d). In the few outcrops in which conglomerates were observed,
317 representing the coarsest fraction of the Pennant Formation, reconstructed flow velocities are greater

318 (>1.9 m s⁻¹) and show greater variation (1.9–2.3 m s⁻¹) while Q₀ is a factor of 1.5–2 greater than in the
319 sand fraction (blue crosses, Fig. 6).

320 Palaeocurrent rose diagrams were produced for each locality using structural measurements of cross-
321 set lee faces, unfolded to account for the dip of beds (Figure 7). A range of palaeocurrent directions
322 were recovered with flow directions to the west more common (11/18 sites) than flow directions to
323 the east. It is important to stress, however, that outcrops belonging to each member would not have
324 necessarily formed part of a single fluvial system, as deposition in the Pennant clearly involved more
325 than one river system in both temporal and spatial senses.

326 Spatial variation of S between outcrops of the same member shows more marked trends, despite the
327 fact that the interquartile ranges of predictions overlap (Figure 8). The clearest of these trends can be
328 seen in the Brithdir Member's three field sites, which show a westward decline in channel gradient
329 from ~6 ×10⁻⁴ in the east to ~4 ×10⁻⁴ in the west. Two sample Kolmogorov-Smirnov tests on the
330 distributions of palaeoslopes resolved at each of the field sites of the Brithdir confirm the sites produce
331 distributions that are significantly different from one another (Supplement 5). It is noted that the
332 Pembrokeshire Pennant, which is here correlated with the Rhondda Member, has significantly steeper
333 palaeoslopes of 5-6 ×10⁻⁴ than the Rhondda outcrops in the west of the South Wales Coalfield.
334 Consequently, the palaeogeographic relationship of these outcrops to the main part of the Pennant
335 remains unclear, as previous authors have noted (e.g., Jones 1977; Jones and Hartley 1993).

336 **Planform morphologies**

337 Plausible estimates of the channel width of single threads in the Pennant Formation, W_C, and the
338 channel belt width, W, are shown in Figure 9a. Mean W_C is 55 m and ranges from 12–106 m. In
339 contrast, values of W using the channel body aspect ratio of Jones (1977) have a mean value of 137
340 m, while outcrop widths measured in this study have a mean value of ca. 210 m. Bankfull water
341 discharges, Q_{bf}, calculated using W_C, have an interquartile range of 80–200 m³ s⁻¹ and a median of 140
342 m³ s⁻¹ (Figure 9b). Considering the entire channel belt, bankfull discharges using the outcrop width
343 give an interquartile range of 440–760 m³ s⁻¹ and a median of 560 m³ s⁻¹ (Figure 9c), while using the
344 ratio of Jones (1977) gives an interquartile range of 320–490 m³ s⁻¹ and a median bankfull discharge
345 of 400 m³ s⁻¹ (Figure 9d).

346 A key question is whether Pennant rivers were single-thread or multi-thread. Figure 10 shows the
347 inverse of channel aspect ratio (i.e., H/W as opposed to W/H) plotted against S/Fr for n = 1227
348 measured cross-sets with corresponding single-thread widths, and for n = 1569 cross-sets with
349 corresponding outcrop widths. For all data points combined (n = 2820), only 0.3% of data points fall

350 outside of the single-thread field of Parker (1976); however, this method has been recently recognised
351 to disfavour multi-thread classification for geologic examples (c.f. Lyster et al. 2022).

352 Here, using the revised stability fields of Lyster et al. (2022), 94% of points calculated using the width
353 scaling method of Greenberg et al. (2021) plot in the revised single-thread stability field of Lyster et
354 al. (2022; Figure 9), which is expected as this method (Equation 6) recovers estimates of single-thread
355 channel widths. Given that single thread widths appear to have been of order 50 m and that outcrop
356 widths have mean values of ~200 m, but maximum values up to 300 m, it is reasonable to anticipate
357 that multiple threads could have coexisted within channel belts. This is consistent with the observation
358 that 90% of data points using our measured outcrop width, which give an upper limit on maximum
359 channel active width, plot in the multi-thread stability field of Lyster et al. (2022). Ultimately, we do
360 not know whether multiple threads were present. However, if present, it is likely that a few active
361 threads existed rather than many active threads, given the relative magnitudes of bar clinofrom
362 widths, thread widths and outcrop widths (e.g., Greenberg et al. 2021). Further, if multiple threads
363 coexisted then, using the y-axis of the multi-thread stability field proposed by Lyster et al. (2022),
364 Pennant rivers were more likely to have been anastomosing multi-thread rivers than braided multi-
365 thread rivers (Figure 9).

366 These results underline that reconstruction of channel planform depends on effective evaluation of
367 channel width estimates alongside facies-based interpretations. Nevertheless, the results presented
368 here suggest that both single-thread and anastomosing multi-thread planforms may have prevailed
369 during Pennant deposition. Therefore, these results do not support the notion that the Pennant
370 Formation preserves predominantly braided multi-thread systems (Kelling 1974; Jones and Hartley
371 1993).

372 **Discussion**

373 **What did the rivers of the Pennant Sandstone look like?**

374 This study provides the first application of a quantitative palaeohydrological framework to the upper
375 Carboniferous rivers of the Pennant Formation, based on a combination of bedform scale
376 measurements, grain size and channel architectural elements. Rivers of the Pennant had individual
377 threads with bankfull widths of ~50 m while channel belts spanned 100–300 m. Median flow depths
378 were 2–3 m, implying median bankfull discharges of 390–560 m³ s⁻¹ across the channel belt. Channel
379 morphodynamics and hydrodynamics remain similar up-section, within the propagated uncertainties,
380 although channels were likely steeper in the Pennant of Pembrokeshire where conglomerates are
381 more abundant and Variscan deformation is more pronounced. Channels with depths of 10 to 15 m

382 were not reconstructed and no measured cross-sets that might suggest such large depths were
383 observed.

384 This study finds that, although the ancient rivers of the Pennant Sandstone drained northwards from
385 the Variscan Mountains in the South (Jones and Hartley 1993; Evans 2004), field results from most
386 localities (11/18) suggest west-directed palaeoflow, matching the study of Jones (1977). Axial drainage
387 is common in foreland basins and can be seen in the modern Ganges Basin, at the foot of the
388 Himalayas, or the rivers of the upper Amazon Basin (Garcia-Castellanos 2002). Flow to the north would
389 have been limited spatially by the presence of the Wales-Brabant High at the northern margin of the
390 foreland basin (Opluštil and Cleal 2007). The landscape was relatively flat in the foreland with river
391 gradients of $4\text{--}5 \times 10^{-4}$ ($0.02\text{--}0.03^\circ$), comparable to upper reaches of the continental Guadalquivir
392 River, southern Spain, ($S = 3.9 \times 10^{-4}$; Baena-Escudero et al. 2016) and of the Ebro River, Northern Spain
393 ($S = 6.7 \times 10^{-4}$; Ollero Ojeda 1990).

394 While previous work on the Pennant produced estimates for channel depths of 10-15 m (Jones 1977),
395 our analyses suggest that rivers of the Rhondda Member were likely 5 times shallower than this. Our
396 data also suggests that planform channel belt widths were 3-8 times narrower than those resolved by
397 Jones (1977). Architectural elements unambiguously related to individual channels and large enough
398 to reflect rivers of the previously reconstructed size were not observed in our field study but
399 amalgamated sandstone packages were observed to reach scales comparable to those previously
400 reported. As such, our results provide constraints between insights that can be drawn from the
401 bedform scale compared to the channel body scale. Jones and Hartley's (1993) study on the reservoir
402 characteristics of the Pennant Sandstone presents a channel depth to width ratio of 1:5–15 based on
403 channel fill deposits while we find a single-thread depth to width ratio of 1:15–30, greater by a factor
404 of ~ 2 , again based on depths derived from cross-set analysis.

405 Within the channel sandstones of the Pennant, distinct horizons of wood (*Lepidodendron* and
406 *Calamites*) debris are observed. These packages resemble clast-supported deposits in places with
407 wood fossils up to 1 m in length found in outcrops of the Llynfi Member (Figure 11). This, along with
408 the presence of coal seams at all stratigraphic intervals of the Pennant, provides evidence of a heavily
409 vegetated region. This is in agreement with the palaeofloral work of Opluštil and Cleal (2007) where
410 an ever-wet, tropical palaeoclimate is proposed. The presence of these wood debris dominated beds
411 in the Pennant indicates rivers displayed marked discharge variability as is also hypothesized in the
412 thesis of Jones (1977). Conglomeratic lags in several outcrops of the Pennant, where reconstructed
413 flow velocities are 1.5-2 times greater than in sands, likely reflect flow dynamics of the largest
414 discharge events that would have occurred in rivers of the upper Carboniferous South Wales foreland

415 basin. In the Westphalian, Britain was palaeogeographically sub-equatorial (Scotese 2001) meaning
416 tectono-climatic conditions may have been analogous to the modern Amazon and Congo basins. Given
417 water discharges of 300–600 m³ s⁻¹ it is estimated that the ancient rivers had drainage areas of 4500–
418 9500 km², based on an average precipitation rate of 2 m yr⁻¹ from modern equatorial rainforests (e.g.,
419 Amazon Rainforest; Sombroek 2001), and assuming water discharge scales with drainage area.

420 Various planforms likely existed over the course of these ancient rivers. Using outcrop widths as a
421 proxy for channel belt widths, many of these rivers may have been multi-threaded. Of these multi-
422 thread rivers, quantitative analysis using estimates of slope and Froude number (Equations 3 and 5),
423 and the stability fields of Lyster et al. (2022), suggest that multi-thread Pennant rivers were likely to
424 have been anastomosing. There is, however, both facies-based and quantitative evidence for single-
425 thread reaches in Pennant rivers. Facies evidence includes laterally dipping accretion surfaces
426 representing meander growth while the correspondence between estimates of single-thread widths
427 and outcrop widths for some localities of the Hughes and Llynfi Members also suggests some outcrops
428 preserve rivers with a single-thread planform. In addition, the variability in resolved palaeocurrent
429 between field sites of similar spatio-temporal setting in the Pennant may suggest that the sinuosity of
430 the rivers was higher than previously reported.

431 The anastomosing river planform morphologies implied by the results in this study suggest that
432 Pennant rivers were likely more stable than previous interpretations of relatively proximal braided
433 systems. Anastomosing rivers are often characterised by large, typically vegetated, mid-channel bars
434 or islands, in contrast to the highly mobile barforms that are typically observed in braided systems
435 (e.g., Makaske 2001). The abundant vegetation in the Variscan foreland in the Westphalian (Opluštil
436 and Cleal 2007) would have acted as a stabilising agent for the river systems, generating the large, but
437 spatially limited, sandstone bodies that occur between the extensive mudstone dominated landscapes
438 in the valleys of South Wales. Overall, results suggest that the hydrodynamics of fluvial systems in the
439 Variscan foreland were remarkably similar throughout Pennant deposition, despite the 10 km Myr⁻¹
440 northward advancement of the Variscan Mountains (Burgess and Gayer 2000) with rivers showing
441 limited temporal trends up-section.

442 Upstream to downstream trends, however, are more visible in the data, particularly for slope; in the
443 Brithdir Member, slope decreases from $\sim 6 \times 10^{-4}$ to 4×10^{-4} across the >10 km plan view distance
444 between three field sites. Considering these trends in palaeoslopes, it is hypothesized here that the
445 three field sites visited in the Brithdir Member sites formed part of the same fluvial system, based on
446 slope, palaeocurrent and the authors' observations of similar facies. The three westernmost localities
447 in the Rhondda Member in the South Wales Coalfield also show decreasing S downstream although

448 the facies evidence is less convincing that they comprise the same system here. The Llynfi and Hughes
449 members do not have field sites showing evidence of being part of the same system and, given the
450 spatial scale (>100 km), are interpreted as outcrops representing spatially separated but temporally
451 equivalent river systems.

452 The mean hydrodynamic parameters and morphologies of Pennant rivers are summarised in Figure
453 12. Figure 12 represents the morphology of a hypothetical modern fluvial system, using the
454 parameters reconstructed in this study, which suggest anastomosing morphologies of ~200 m width
455 and ~2.5 m flow depths were most common in the rivers of the Pennant.

456 Overall, results of this study suggest that Pennant rivers exhibited both anastomosing and single-
457 threaded planforms with bankfull discharges up to $560 \text{ m}^3 \text{ s}^{-1}$. To a first order, the rivers were similar
458 in scale and tectonic setting to the modern Guadalquivir and Ebro rivers of Spain, and the upper Kuban
459 River, Russia.

460 **Tectonic implications**

461 The ancient river deposits preserved in the stratigraphy of the Pennant Sandstone provide an
462 opportunity to explore the evolution of the northern foreland basin margin of the Variscan mountain
463 belt. Our data analysis shows that there is no statistical temporal change in the morphodynamic
464 parameters resolved in the Pennant rivers over the approximately 7 Myr depositional interval of the
465 formation, despite a reconstructed northward migration of the Variscan Front of greater than 50 km
466 in the same period (Burgess and Gayer 2000). In contrast, recent quantitative palaeohydrological
467 studies of ancient rivers draining the Sevier fold-and-thrust belt of the Upper Cretaceous of Utah,
468 which flowed in a broadly similar orogenic setting to the Pennant's rivers, show marked steepening
469 temporal trends in palaeoslope over a 9 Myr period relating to the migration of the thrust front (Lyster
470 et al. 2021; Lyster et al., 2022). Rivers of the Pennant Formation appear to be remarkably insensitive
471 to tectonic forcing by comparison.

472 Various mechanisms could be responsible for this stability in reconstructed palaeoslopes. Firstly,
473 subsidence rates of approximately $130\text{-}260 \text{ m Myr}^{-1}$ in the centre of the South Wales basin (Burgess
474 and Gayer 2000) may have been neatly balanced by sediment supply from Pennant rivers, maintaining
475 the fluvial topography of the depocenter despite the advancing thrust front, which continued to
476 migrate until 305 Ma, after the end of Pennant deposition. In this explanation our sample sites are
477 hypothesised to be sufficiently downstream within the basin that we do not capture any steepening
478 palaeoslopes of feeder rivers located to the South. Instead our data capture, in relative terms, a
479 topographic steady-state within the fluvial fill of the basin despite the evolving tectonic context. One

480 potentially important influence on the slopes of the foreland that has not as yet been explored, is the
481 presence of the Wales-Brabant High bounding the North of the basin (Figure 1c) which would act as a
482 secondary source of the sediment for the rivers of the Pennant. This contribution from the north is
483 consistent with the spread in palaeoflow directions presented earlier (Figure 7). This palaeogeography
484 creates a pronounced contrast in tectonic setting to the Upper Cretaceous rivers of the Sevier fold-
485 and-thrust belt that drained directly into the Western Interior Seaway (Lyster et al. 2021) and
486 additional sediment supply from the Wales-Brabant High thus would also have helped to offset any
487 slope increases. Finally, we must also acknowledge that climatic forcing can also influence the
488 morphodynamics of rivers, with slope and sediment supply variations also being coupled directly to
489 river discharge. The presence of abundant vegetation on the banks of the rivers could have acted as
490 a stabilising agent against tectonic forcing. Palaeoclimatic reconstructions (e.g., Opluštil and Cleal
491 2007) however, do not propose significant local climatic variations in the Westphalian and as our data
492 analyses do not show a uni-directional change in palaeohydrological variables or in water discharge,
493 we therefore suggest that the morphodynamics of the Pennant's rivers reflect an equilibrium between
494 accommodation generation and sediment supply within the foreland basin setting.

495 **Future perspectives and challenges**

496 Dominantly qualitative approaches have produced valuable insights into the hydrodynamics of the
497 ancient rivers of the Pennant (e.g., Kelling 1974; Jones 1977; Jones and Hartley 1993) but the methods
498 presented in this study show that a well-constrained quantitative framework can be used to determine
499 hydrodynamic and morphological parameters using easily measurable field data (e.g., cross set
500 heights). This is particularly pertinent where poor outcrop preservation limits architectural mapping
501 but cross sets and grain sizes can be measured. However, it remains critical to consider qualitative and
502 facies-based evidence together where available to validate quantitative reconstructions (e.g.,
503 Supplement 3). The combination of methodologies used in this study demonstrates how to tackle this
504 issue in the rock record. Here, reconstructions of hydrodynamics using cross-set and grain size
505 measurements (Leclair and Bridge 2001; Trampush et al. 2014; Bradley and Venditti 2017) are found
506 to provide results in agreement with evidence and observations of, for instance, the heights of
507 accretion packages. The reconstruction of anastomosing and single thread planforms is consistent
508 with facies associations and bedforms previously documented in the Pennant Sandstone (Kelling 1969,
509 1974; Jones and Hartley 1993) but the data in this work also allow us to rule out some reconstructions
510 such as channel depths as great as 15 m (c.f. Jones 1977), which are inconsistent with the scale of the
511 dune-scale cross-set heights, and the implied original bedform heights, documented here. Recent
512 theoretical work has continued to improve extraction of quantitative information from fluvial strata

513 (e.g., Greenberg et al. 2021; Lyster et al. 2022) and further refinements will facilitate reconstructions
514 in a broader number of ancient fluvial systems to greater resolution than previously possible.

515 As all the equations used in this study carry forward calculated parameters (e.g., slope calculations
516 implement the previously calculated flow depths), errors and uncertainties are compounded in this
517 type of analysis. This must be addressed carefully and, here, we use a Monte Carlo uncertainty
518 approach to propagate error throughout. Despite this, the greatest confidence remains in parameters
519 calculated early in the methodology, due to the potential for architectural validation (i.e., H) while
520 uncertainty is greater in parameters calculated later in the workflow which require more assumptions
521 to be made (i.e., Q_{bf}).

522 Moving beyond the scope of this study, further detailed work is required to identify and trace
523 individual fluvial systems in the Pennant Sandstone, which will serve to better constrain upstream to
524 downstream trends in these rivers and to constrain the pathways of sediment dispersal from the
525 Variscan highlands in the south. Additionally, previous interpretations of wet climatic conditions
526 throughout Pennant deposition, as well as the presence of conglomeratic channel fills and woody
527 debris pointing to the occurrence of floods, could be used to better constrain potential
528 palaeohydrological variability in these systems and the climate drivers behind this (Fielding et al. 2018;
529 Leary and Ganti 2020). Assuming uncertainties are appropriately acknowledged, there is clear
530 potential to apply the methodology used in this study to many more ancient fluvial systems on Earth,
531 but also increasingly on other planetary surfaces including Mars, where high resolution imagery
532 increasingly enables grain-sizes, bedforms, and larger scale architectures to be quantified (e.g., Edgar
533 et al. 2018; Davis et al. 2019; Stack et al. 2019; Balme et al. 2020; Mangold et al. 2021).

534 **Conclusion**

535 During the Westphalian stage of the Upper Carboniferous, the Variscan foreland in South Wales was
536 characterised by large fluvial systems with median bankfull discharges of $390\text{--}560\text{ m}^3\text{ s}^{-1}$, that
537 deposited over 1300 m of sediment over a period of approximately 4 Myr. The reconstruction of the
538 ancient fluvial systems of the Pennant Formation presented in this study suggests these rivers had
539 median flow depths of 2–3 m, median slopes of $4\text{--}5 \times 10^{-4}$ (m/m), individual channel thread widths of
540 a few tens of metres, and channel belt widths of 100–200 m — these ancient rivers likely possessed
541 both anastomosing and single-thread reaches. The reconstructed depositional setting is consistent
542 with modern rivers in similar tectonic regimes such as the Ebro and Guadalquivir rivers, Spain, and in
543 climatically similar regions such as the upper Amazon Basin. There is little variation in these key
544 palaeohydrological and morphodynamic variables up-section through the five members of the
545 Pennant.

546 This study provides new insights into river behaviour during the latter stages of supercontinent
547 assembly. Despite rapid subsidence rates in the South Wales foreland basin, little temporal variation
548 is observed in key hydrodynamics and morphodynamics up-section, which implies these ancient fluvial
549 systems were relatively stable in a time of intense compressional tectonism. This study of
550 Carboniferous rivers in the UK adds to the growing body of recent work applying quantitative
551 techniques to fluvial strata (e.g., Ganti et al. 2019; Lyster et al. 2021) and builds on the qualitative and
552 facies-based fluvial sedimentological studies undertaken on the Pennant Sandstone. This work
553 demonstrates the utility of reconstructing hydrodynamics and styles of ancient fluvial systems from
554 quantitative field data and could be applied even where facies-based reconstructions are equivocal or
555 where outcrop is limited.

556 **Acknowledgements**

557 The authors acknowledge research support from Imperial College London. We thank Gary Hampson
558 and Cedric John for useful feedback on an early version of the manuscript and the reviewers and editor
559 for their comments on the manuscript. This feedback has resulted in a much improved study.

560 **Author contributions**

561 **JW:** Data curation (lead), formal analysis (lead), investigation (lead), methodology (lead), visualization
562 (lead), writing – original draft (lead), writing – review and editing (equal); **JM:** Data curation
563 (supporting), investigation (supporting), writing – review and editing (supporting); **SL:** Data curation
564 (supporting), formal analysis (supporting), investigation (supporting), methodology (supporting),
565 supervision (equal), writing – review and editing (equal); **AW:** Data curation (supporting), formal
566 analysis (supporting), investigation (supporting), methodology (supporting), supervision (equal),
567 writing – review and editing (equal).

568 **Data availability**

569 All data generated or analysed during this study are included in this published article (and its
570 supplementary information files).

571 **References**

- 572 Allen, J.R.L., 1963. The classification of cross-stratified units, with notes on their origin.
573 *Sedimentology*, 2: 93–114.
- 574
- 575 Allmendinger, R. 2020. *Stereonet 11*.
576 <http://www.geo.cornell.edu/geology/faculty/RWA/programs/stereonet.html>

577

578 Baena-Escudero, R., Guerrero-Amador, I., García-Martínez, B., & Carlos Posada-Simeón, J. 2016.
579 Human activities and inundation risks in the plain of the Guadalquivir River (in the reach between
580 palma del río and seville, spain). *Boletín de La Asociación de Geógrafos Españoles* , 72, 572–534.

581

582 Balme, M. R., Gupta, S., Davis, J. M., Fawdon, P., Grindrod, P. M., Bridges, J. C., Sefton-Nash, E., &
583 Williams, R. M. E. 2020. Aram Dorsum: An Extensive Mid-Noachian Age Fluvial Depositional System
584 in Arabia Terra, Mars. *Journal of Geophysical Research: Planets*, 125(5).

585 <https://doi.org/10.1029/2019JE006244>.

586

587 Barclay, W.J. 2011. Geology of the Swansea district – a brief explanation of the geological map. *Sheet*
588 *Explanation of the British Geological Survey*. 1:50,000 Sheet 247 Swansea (England and Wales).

589

590 Bhattacharya, J. P., & Tye, R. S. 2004. Searching for Modern Ferron Analogs and Application to
591 Subsurface Interpretation. In *Regional to Wellbore Analog for Fluvial-Deltaic Reservoir Modeling: The*
592 *Ferron Sandstone of Utah* (Vol. 50, pp. 39–57). American Association of Petroleum Geologists.

593

594 Bhattacharya, J. P., Copeland, P., Lawton, T. F., & Holbrook, J. 2016. Estimation of source area, river
595 paleo-discharge, paleoslope, and sediment budgets of linked deep-time depositional systems and
596 implications for hydrocarbon potential. *Earth-Science Reviews*, 153, 77–110.

597 <https://doi.org/10.1016/j.earscirev.2015.10.013>

598

599 Bradley, R. W., & Venditti, J. G. 2017. Reevaluating dune scaling relations. In *Earth-Science Reviews*
600 (Vol. 165, pp. 356–376). Elsevier B.V. <https://doi.org/10.1016/j.earscirev.2016.11.004>

601

602 Bridge, J. S., & Mackey, S. D. 1992. A Theoretical Study of Fluvial Sandstone Body Dimensions. In *The*
603 *Geological Modelling of Hydrocarbon Reservoirs and Outcrop Analogues* (pp. 213–236). John Wiley &
604 Sons, Ltd. <https://doi.org/https://doi.org/10.1002/9781444303957.ch14>

605

606 Bridgland, D.R., Bennett, J.A., McVicar-Wright, S.E. & Scrivener, R.C. 2014. Rivers through geological
607 time: the fluvial contribution to understanding our planet. *Proceedings of the Geologists’*
608 *Association*, 125 (5-6). pp. 503-510. <https://doi.org/10.1016/j.pgeola.2014.11.001>

609

610 Brierley, G. J. 1989. River planform facies models: the sedimentology of braided, wandering and
611 meandering reaches of the Squamish River, British Columbia. *Sedimentary Geology*, 61(1), 17–35.
612 [https://doi.org/10.1016/0037-0738\(89\)90039-0](https://doi.org/10.1016/0037-0738(89)90039-0)
613

614 Burgess, P. M., & Gayer, R. A. 2000. Late Carboniferous tectonic subsidence in South Wales:
615 implications for Variscan basin evolution and tectonic history in SW Britain. *Journal of the Geological*
616 *Society*, 157, 93-104, <https://doi.org/10.1144/jgs.157.1.93>
617

618 Castellort, S., Goren, L., Willett, S. D., Champagnac, J. D., Herman, F., & Braun, J. 2012. River
619 drainage patterns in the New Zealand Alps primarily controlled by plate tectonic strain. *Nature*
620 *Geoscience*, 5(10), 744–748. <https://doi.org/10.1038/ngeo1582>
621

622 Chamberlin, E. P., & Hajek, E. A. 2019. Using bar preservation to constrain reworking in channel-
623 dominated fluvial stratigraphy. *Geology*, 47(6), 531–534. <https://doi.org/10.1130/G46046.1>
624

625 Chow, V.T., 1959, Open-channel hydraulics: New York, McGraw-Hill Book Co., 680p
626 Cleal, C. J., & Thomas, B. A. 1992. Lower Westphalian D fossil plants from the Nolton-Newgale Coalfield, Dyfed
627 (Great Britain). *Geobios*, 25(3), 315–322. [https://doi.org/10.1016/0016-6995\(92\)80002-U](https://doi.org/10.1016/0016-6995(92)80002-U)
628

629 Davis, J. M., Gupta, S., Balme, M., Grindrod, P. M., Fawdon, P., Dickeson, Z. I., & Williams, R. M. E.
630 2019. A Diverse Array of Fluvial Depositional Systems in Arabia Terra: Evidence for mid-Noachian to
631 Early Hesperian Rivers on Mars. *Journal of Geophysical Research: Planets*, 124(7), 1913–1934.
632 <https://doi.org/10.1029/2019JE005976>
633

634 Davydov V.I., Korn D., Schmitz M.D., Gradstein F.M. and Hammer O. 2012. The Carboniferous Period.
635 In: Gradstein F.M., Ogg J.G., Schmitz M.D. and Ogg G.M. (eds) The Geologic Time Scale 2012, Volume
636 2. Elsevier, Amsterdam, 603–651.
637

638 De la Beche, Sir H. 1846. On the formation of rocks of South Wales and South Western England.
639 Memoirs of the Geological Survey. 1. 1-296.
640

641 Duller, R. A., Whittaker, A. C., Fedele, J. J., Whitchurch, A. L., Springett, J., Smithells, R., Fordyce, S., &
642 Allen, P. A. 2010. From grain size to tectonics. *Journal of Geophysical Research: Earth Surface*, 115(3).
643 <https://doi.org/10.1029/2009JF001495>

644

645 Edgar, L. A., Gupta, S., Rubin, D. M., Lewis, K. W., Kocurek, G. A., Anderson, R. B., Bell, J. F., Dromart,
646 G., Edgett, K. S., Grotzinger, J. P., Hardgrove, C., Kah, L. C., Leveille, R., Malin, M. C., Mangold, N.,
647 Milliken, R. E., Minitti, M., Palucis, M., Rice, M., ... Williams, A. J. 2018. Shaler: in situ analysis of a
648 fluvial sedimentary deposit on Mars. *Sedimentology*, 65(1), 96–122.
649 <https://doi.org/10.1111/sed.12370>

650

651 Eriksson, P. G., Bumby, A. J., Brümer, J. J., & van der Neut, M. 2006. Precambrian fluvial deposits:
652 Enigmatic palaeohydrological data from the c. 2–1.9 Ga Waterberg Group, South Africa. *Sedimentary
653 Geology*, 190(1), 25–46. <https://doi.org/10.1016/j.sedgeo.2006.05.003>

654

655 Evans, B. G. 2004. An introduction to the South Wales Pennant Formation: its origin, outcrop and
656 conservation. *Geologica Balcanica*, 34.

657

658 Fielding, C. R., Alexander, J., & Allen, J. P. (2018). The role of discharge variability in the formation
659 and preservation of alluvial sediment bodies. In *Sedimentary Geology* (Vol. 365, pp. 1–20). Elsevier
660 B.V. <https://doi.org/10.1016/j.sedgeo.2017.12.022>

661

662 Ganti, V., Lamb, M. P., & McElroy, B. 2014. Quantitative bounds on morphodynamics and
663 implications for reading the sedimentary record. *Nature Communications*, 5.
664 <https://doi.org/10.1038/ncomms4298>

665

666 Ganti, V., Whittaker, A. C., Lamb, M. P., & Fischer, W. W. 2019. Low-gradient, single-threaded rivers
667 prior to greening of the continents. *Proceedings of the National Academy of Sciences of the United
668 States of America*, 116(24), 11652–11657. <https://doi.org/10.1073/pnas.1901642116>

669

670 Garcia-Castellanos, D. 2002. Interplay between lithospheric flexure and river transport in foreland
671 basins. *Basin Research*, 14(2), 89–104. <https://doi.org/10.1046/j.1365-2117.2002.00174.x>

672

673 Gayer, R., & Jones, J. 1989. The Variscan foreland in south Wales. *Proceedings of the Ussher Society*,
674 7(2), 177–179.

675

676 Gayer, R., & Pesek, J. 1992. Cannibalisation of coal measures in the south wales coalfield-significance
677 for foreland basin evolution. *Proceedings of the Ussher Society*, 8, 44-49

678
679
680
681
682
683
684
685
686
687
688
689
690
691
692
693
694
695
696
697
698
699
700
701
702
703
704
705
706
707
708
709
710
711

Gibling, M., & Davies, N. 2021. Palaeozoic landscapes shaped by plant evolution. *Nature Geosci* 5, 99–105. <https://doi.org/10.1038/ngeo1376>

Greenberg, E., Ganti, V., & Hajek, E. 2021. Quantifying bankfull flow width using preserved bar clinofolds from fluvial strata. *Geology*, 49(9), 1038–1043. <https://doi.org/10.1130/G48729.1>

Hack, J. T. 1957. Studies of longitudinal stream profiles in Virginia and Maryland. *Shorter Contributions to General Geology 1956*, 294(B), 45-97 <https://doi.org/10.3133/pp294B>

Hajek, E. A., & Heller, P. L. 2012. Flow-depth scaling in alluvial architecture and nonmarine sequence stratigraphy: Example from the Castlegate Sandstone, Central Utah, U.S.A. *Journal of Sedimentary Research*, 82(2), 121–130. <https://doi.org/10.2110/jsr.2012.8>

Harries, R. M. et al. 2021. Impact of climate on landscape form, sediment transfer and the sedimentary record. *Earth Surface Processes and Landforms* (2021) <https://doi.org/10.1002/esp.5075>.

Hartley, A. J., & Warr, L. N. 1990. Upper Carboniferous foreland basin evolution in SW Britain. *Proceedings of the Ussher Society*, 7(3), 212–216.

Hjellbakk, A. 1997. Facies and fluvial architecture of a high-energy braided river: the Upper Proterozoic Segloddan Member, Varanger Peninsula, northern Norway. *Sedimentary Geology*, 114(1), 131–161. [https://doi.org/10.1016/S0037-0738\(97\)00075-4](https://doi.org/10.1016/S0037-0738(97)00075-4)

Holbrook, J., & Wanas, H. 2014. A fulcrum approach to assessing source-to-sink mass balance using channel paleohydrologic parameters derivable from common fluvial data sets with an example from the Cretaceous of Egypt. *Journal of Sedimentary Research*, 84(5), 349–372.

<https://doi.org/10.2110/jsr.2014.29>

Ielpi, A., Rainbird, R. H., Ventra, D., & Ghinassi, M. 2017. Morphometric convergence between Proterozoic and post-vegetation rivers. *Nature Communications*, 8(1), 15250.

<https://doi.org/10.1038/ncomms15250>

712 Jenkins, T. B. 1962. The Sequence and Correlation of the Coal Measures of Pembrokeshire. *Quarterly*
713 *Journal of the Geological Society of London*. 118, 65-101.
714

715 Jones, C. M. 1977. The sedimentology of Carboniferous fluvial and deltaic sequences; the Roaches
716 Grit Group of the south-west Pennines and the Pennant Sandstone of the Rhondda Valleys. *PhD*
717 *Thesis*.
718

719 Jones, J. A. 1991. A mountain front model for the Variscan deformation of the South Wales coalfield.
720 *Journal of the Geological Society*, 148(5), 881 LP – 891. <https://doi.org/10.1144/gsjgs.148.5.0881>
721

722 Jones, J. A., & Hartley, A. J. 1993. Reservoir characteristics of a braid-plain depositional system: the
723 Upper Carboniferous Pennant Sandstone of South Wales. *Geological Society, London, Special*
724 *Publications*, 73(1), 143 LP – 156. <https://doi.org/10.1144/GSL.SP.1993.073.01.09>
725

726 Julien, P. Y., & Klaassen, G. J. 1995. Sand-dune geometry of large rivers during floods. *Journal of*
727 *Hydraulic Engineering*, 121(9), 657–663. [https://doi.org/10.1061/\(ASCE\)0733-9429\(1995\)121:9\(657\)](https://doi.org/10.1061/(ASCE)0733-9429(1995)121:9(657))
728

729 Kelling, G. 1969. The environmental significance of cross stratification parameters in an upper
730 Carboniferous fluvial basin. *Journal of Sedimentary Research*, 39(3), 857–875.
731 <https://doi.org/10.1306/74D71D52-2B21-11D7-8648000102C1865D>
732

733 Kelling, G. 1974. Upper Carboniferous sedimentation in South Wales. In T. R. Owen (Ed.), *The Upper-*
734 *Palaeozoic and Post-Palaeozoic rocks of Wales*, 185–225. University of Wales Press.
735

736 Leary, K. C. P., & Ganti, V. 2020. Preserved Fluvial Cross Strata Record Bedform Disequilibrium
737 Dynamics. *Geophysical Research Letters*, 47(2). <https://doi.org/10.1029/2019GL085910>
738

739 Leclair, S. F., & Bridge, J. S. 2001. Quantitative Interpretation of Sedimentary Structures Formed by
740 River Dunes. *Journal of Sedimentary Research*; 71 (5): 713–716. [https://doi.org/10.1306/2DC40962-](https://doi.org/10.1306/2DC40962-0E47-11D7-8643000102C1865D)
741 [0E47-11D7-8643000102C1865D](https://doi.org/10.1306/2DC40962-0E47-11D7-8643000102C1865D)
742

743 Leopold, L. B., & Maddock Jr., T. 1953. The hydraulic geometry of stream channels and some
744 physiographic implications. *USGS Numbered Series Professional Paper*. 252.
745 <https://doi.org/10.3133/pp252>
746

747 Leopold, L. B., & Wolman, M. G. 1960. River meanders. *Geological Society of America Bulletin*, 71(6),
748 769–793. [https://doi.org/10.1130/0016-7606\(1960\)71\[769:RM\]2.0.CO;2](https://doi.org/10.1130/0016-7606(1960)71[769:RM]2.0.CO;2)
749

750 Leveridge, B., & Hartley, A. J. 2006. The Variscan Orogeny : the development and deformation of
751 Devonian/Carboniferous basins in SW England and South Wales. In P. J. Brenchley & P. F. Rawson
752 (Eds.), *The Geology of England and Wales* (pp. 225–255). Geological Society of London.
753

754 Li, Y., Bhattacharya, J. P., Ahmed, S., & Garza, D. 2018. Re-evaluating the paleogeography of the
755 river-dominated and wave-influenced Ferron notom delta, Southern central Utah: An integration of
756 detailed facies-architecture and paleocurrent analysis. *Journal of Sedimentary Research*, 88(2), 214–
757 240. <https://doi.org/10.2110/jsr.2018.9>
758

759 Lyster, S. J., Whittaker, A. C., Allison, P. A., Lunt, D. J., & Farnsworth, A. 2020. Predicting sediment
760 discharges and erosion rates in deep time—examples from the late Cretaceous North American
761 continent. *Basin Research*, 32(6), 1547–1573. <https://doi.org/10.1111/bre.12442>
762

763 Lyster, S. J., Whittaker, A. C., Hampson, G. J., Hajek, E. A., Allison, P. A., & Lathrop, B. A. 2021.
764 Reconstructing the morphologies and hydrodynamics of ancient rivers from source to sink:
765 Cretaceous Western Interior Basin, Utah, USA. *Sedimentology*, n/a(n/a).
766 <https://doi.org/10.1111/sed.12877>
767

768 Lyster, S.J., Whittaker, A.C. and Hajek, E.A. 2022, Accepted. The problem of Paleo-planforms.
769 *Geology*
770

771 Mahon, R.C. and McElroy, B. 2018. Indirect estimation of bedload flux from modern sand-bed rivers
772 and ancient fluvial strata. *Geology*, 46(7), 579–582, <https://doi.org/10.1130/G40161.1>
773

774 Makaske, B. 2001. Anastomosing rivers: a review of their classification, origin and sedimentary
775 products. *Earth-Science Reviews* (Vol. 53). [https://doi.org/10.1016/S0012-8252\(00\)00038-6](https://doi.org/10.1016/S0012-8252(00)00038-6)
776

777 Mangold, N., Gupta, S., Gasnault, O., Dromart, G., Tarnas, J. D., Sholes, S. F., Horgan, B., Quantin-
778 Nataf, C., Brown, A. J., Mouélic, S. L., Yingst, R. A., Bell, J. F., Beyssac, O., Bosak, T., Calef, F., Ehlmann,
779 B. L., Farley, K. A., Grotzinger, J. P., Hickman-Lewis, K., ... Williford, K. H. 2021. Perseverance rover
780 reveals an ancient delta-lake system and flood deposits at Jezero crater, Mars. *Science*, 374(6568).
781 <https://doi.org/10.1126/science.abl4051>
782

783 Manning, R., Griffith, J. P., Pigot, T. F., & Vernon-Harcourt, L. F. 1890. On the flow of water in open
784 channels and pipes. *Transactions of the Institution of Civil Engineers of Ireland*. Vol XX, 161-207.
785

786 Miall, A. D. 1985. Architectural-element analysis: A new method of facies analysis applied to fluvial
787 deposits. *Earth-Science Reviews*, 22(4), 261–308. [https://doi.org/10.1016/0012-8252\(85\)90001-7](https://doi.org/10.1016/0012-8252(85)90001-7)
788

789 Michael, N. A., Whittaker, A. C., Carter, A. & Allen, P. A. 2014. Volumetric budget and grain-size
790 fractionation of a geological sediment routing system: Eocene Escanilla Formation, south-central
791 Pyrenees. *GSA Bulletin* 126, 585–599. <https://doi.org/10.1130/B30954.1>
792

793 Mohrig, D., Heller, P. L., Paola, C., & Lyons, W. J. 2000. Interpreting avulsion process from ancient
794 alluvial sequences: Guadalupe-Matarranya system (northern Spain) and Wasatch Formation
795 (western Colorado). *GSA Bulletin*, 112(12), 1787–1803. [https://doi.org/10.1130/0016-
796 7606\(2000\)112<1787:IAPFAA>2.0.CO;2](https://doi.org/10.1130/0016-7606(2000)112<1787:IAPFAA>2.0.CO;2)
797

798 Ollero Ojeda, A. 1990. Slope, sinuosity and channel patterns in the Ebro river. *Cuadernos de*
799 *Investigación Geográfica*, 16(0), 73. <https://doi.org/10.18172/cig.985>
800

801 Opluštil, S., & Cleal, C. J. 2007. A comparative analysis of some Late Carboniferous basins of Variscan
802 Europe. *Geological Magazine*, 144(3), 417–448. <https://doi.org/10.1017/S0016756807003330>
803

804 Paola, C., & Borgman, L. 1991. Reconstructing random topography from preserved stratification.
805 *Sedimentology*, 38(4), 553–565. <https://doi.org/10.1111/j.1365-3091.1991.tb01008.x>
806

807 Paola, C., & Mohrig, D. 1996. Palaeohydraulics revisited: palaeoslope estimation in coarse-grained
808 braided rivers. *Basin Research*, 8(3), 243–254. <https://doi.org/10.1046/j.1365-2117.1996.00253.x>
809

810 Parker, G. 1976. On the cause and characteristic scales of meandering and braiding in rivers. *Journal*
811 *of Fluid Mechanics*, 76(3), 457–480. <https://doi.org/10.1017/S0022112076000748>
812

813 Plink-Bjorklund, P. 2015. Morphodynamics of rivers strongly affected by monsoon precipitation:
814 Review of depositional style and forcing factors. *Sedimentary Geology*, 323.
815 <https://doi.org/10.1016/j.sedgeo.2015.04.004>
816

817 Rasband, W. S. 2018. *ImageJ*. <https://imagej.nih.gov/ij/>
818

819 Rippon, J. H. 1996. Sand body orientation, palaeoslope analysis and basin-fill implications in the
820 Westphalian A–C of Great Britain. *Journal of the Geological Society*, 153(6), 881–900.
821 <https://doi.org/10.1144/gsjgs.153.6.0881>
822

823 Sadler, P. M. 1981. Sediment Accumulation Rates and the Completeness of Stratigraphic Sections.
824 *The Journal of Geology*, 89(5), 569–584. <https://doi.org/10.1086/628623>
825

826 Scotese, C. R. 2001. Atlas of Earth History, Volume 1, Paleogeography. *PALAEOMAP Project*.
827

828 Sharma, S., Bhattacharya, J. P., & Richards, B. 2017. Source-to-sink sediment budget analysis of the
829 Cretaceous Ferron Sandstone, Utah, U.S.A, using the fulcrum approach. *Journal of Sedimentary*
830 *Research*, 87(6), 594–608. <https://doi.org/10.2110/jsr.2017.23>
831

832 Shibata, K., Adhiperdana, B. G., & Ito, M. 2018. Quantitative reconstruction of cross-sectional
833 dimensions and hydrological parameters of gravelly fluvial channels developed in a forearc basin

834 setting under a temperate climatic condition, central Japan. *Sedimentary Geology*, 363, 69–82.

835 <https://doi.org/10.1016/j.sedgeo.2017.10.014>

836

837 Sombroek, W. 2001. Spatial and temporal patterns of Amazon rainfall: Consequences for the
838 planning of agricultural occupation and the protection of primary forests. *Ambio*, 30(7), 388–396.

839 <https://doi.org/10.1579/0044-7447-30.7.388>

840

841 Stack, K. M., Grotzinger, J. P., Lamb, M. P., Gupta, S., Rubin, D. M., Kah, L. C., Edgar, L. A., Fey, D. M.,
842 Hurowitz, J. A., McBride, M., Rivera-Hernández, F., Sumner, D. Y., van Beek, J. K., Williams, R. M. E.,
843 & Aileen Yingst, R. 2019. Evidence for plunging river plume deposits in the Pahrump Hills member of
844 the Murray formation, Gale crater, Mars. *Sedimentology*, 66(5), 1768–1802.

845 <https://doi.org/10.1111/sed.12558>

846

847 Strahan, A. 1899. The geology of the South Wales Coalfield. Part I. The country around Newport,
848 Monmouthshire. 1st edit. *Memoirs of the Geological Survey*. 249.

849

850 Straub, K. M., Duller, R. A., Foreman, B. Z., & Hajek, E. A. 2020. Buffered, Incomplete, and Shredded:
851 The Challenges of Reading an Imperfect Stratigraphic Record. *Journal of Geophysical Research: Earth*

852 *Surface*, 125(3). <https://doi.org/10.1029/2019JF005079>

853

854 Trampush, S. M., Huzurbazar, S., & McElroy, B. 2014. Empirical assessment of theory for bankfull
855 characteristics of alluvial channels. *Water Resources Research*, 50(12), 9211–9220.

856 <https://doi.org/10.1002/2014WR015597>

857

858 van Rijn, L. C. 1984. Sediment Transport, Part III: Bed forms and Alluvial Roughness. *Journal of*
859 *Hydraulic Engineering*, 110(12), 1733–1754. [https://doi.org/10.1061/\(ASCE\)0733-](https://doi.org/10.1061/(ASCE)0733-)

860 [9429\(1984\)110:12\(1733\)](https://doi.org/10.1061/(ASCE)0733-9429(1984)110:12(1733))

861

862 Waters, C. N., Browne, M. A., Dean, M. T., & Powell, J. H. 2007. Lithostratigraphical framework for
863 Carboniferous successions of Great Britain (Onshore). *British Geological Survey*.

864

865 Waters, C. N., Waters, R. A., Barclay, W. J., & Davies, J. R. 2009. A lithostratigraphical framework for
866 the Carboniferous successions of southern Great Britain (onshore). *British Geological Survey*.

867

868 Wentworth, C. K. 1922. A Scale of Grade and Class Terms for Clastic Sediments. *The Journal of*
869 *Geology*, 30(5), 377–392.

870

871 Whittaker, A. C. 2012. How do landscapes record tectonics and climate? *Lithosphere*, 4(2), 160–164.

872 <https://doi.org/10.1130/RF.L003.1>

873

874 Williams, G. P. 1984. Paleohydrological Methods and Some Examples from Swedish Fluvial
875 Environments II—River Meanders. *Geografiska Annaler: Series A, Physical Geography*, 66(1–2), 89–
876 102. <https://doi.org/10.1080/04353676.1984.11880101>

877

878 Wolman, G. M. 1954. A method of sampling coarse river-bed material. *American Geophysical Union*,
879 35(6).

880

881 Woodland, A. W., Evans, W. B., & Stephens, J. v. 1957. Classification of the Coal Measures of South
882 Wales with special reference to the Upper Coal Measures. *Bulletin of the Geological Survey of Great*
883 *Britain. No. 13.*, 6-13.

884

885 Xu, J., Snedden, J. W., Galloway, W. E., Milliken, K. T., & Blum, M. D. 2017. Channel-belt scaling
886 relationship and application to early Miocene source-to-sink systems in the Gulf of Mexico basin.
887 *Geosphere*, 13(1), 179–200. <https://doi.org/10.1130/GES01376.1>

888

889 Yalin, M. S. 1964. Geometrical Properties of Sand Waves. *Journal of Hydraulic Engineering*, 90, 105–
890 119.

891

892 **Figure Captions**

893 Fig. 1 – (a) Location map showing the extent of the Pennant Sandstone Formation in South Wales,
894 UK. (b) Geological map of the primary study area, the South Wales Coalfield with field sites shown
895 (excludes Pembrokeshire localities). Contains British Geological Survey materials ©UKRI 2021. (c)

896 Simplified paleogeographic reconstruction of England and Wales in the Westphalian Stage. Modified
897 after Burgess and Gayer (2001) and Opluštil and Cleal (2007).

898 Fig. 2 - Stratigraphy of the Pennant Sandstone Formation, correlated across the Neath Disturbance
899 (major N-S trending Caledonoid fault). Major named coal seams are indicated. Approximate
900 stratigraphic interval of this study's field sites also shown. Modified after (Barclay 2011) with age
901 data from BGS Geological Timechart.

902 Fig. 3 - Selected field photographs. **(a-d)** Cross-sets of the Pennant Sandstone (a-b = Rhondda
903 Member, c-d = Brithdir Member). **(b & d)** Interpreted cross-sets in photos **(a & c)**. Cyan lines show
904 where height measurements were taken for distributions, red lines show where cross-set height
905 maxima were measured. **(e)** Grain size photograph of medium sand fraction, D50 = 0.375 mm. **(f)**
906 Grain size photograph of conglomeratic lag in the Pennant Sandstone Formation, D50 = 9 mm.

907 Fig. 4 - Selected photographs and architectural interpretations of field localities of each member of
908 the Pennant Sandstone. Note channel and accretion packages are not distinguished here but
909 package type was noted at each example. **(a & b)** Swansea Member; **(c & d)** Hughes Member; **(e & f)**
910 Brithdir Member; **(g & h)** Rhondda Member; **(i & j)** Llynfi Member.

911 Fig. 5 - Plots of measured mean cross-set height from distributions (n = 268) against maximum cross
912 set heights, separated into **(a)** plot of data from all Pennant Sandstone Formation and **(b)** plot of
913 data separated by member within the formation. Scaling relationships are derived from a linear
914 regression through the origin of the dataset.

915 Fig. 6 - Boxplots of palaeohydrological characteristics of the rivers of the Pennant Sandstone
916 Formation and each of its members. Every cross-set measured in each member is represented in the
917 median and interquartile range of each plot. Conglomerate fraction indicated by blue cross (no
918 conglomerate present in Brithdir Member). Median package height for each member is indicated as
919 green cross on flow depth plots.

920 Fig. 7 - Palaeocurrent rose diagrams using field data from each field site in the **(a)** South Wales
921 Coalfield and **(b)** Pembrokeshire Coalfield. Although there is variability with some northwards
922 directed currents, flow is predominantly to the west in the Pennant Sandstone Formation (11/18
923 localities). It is also unclear if our localities of the same member represent the same fluvial system.

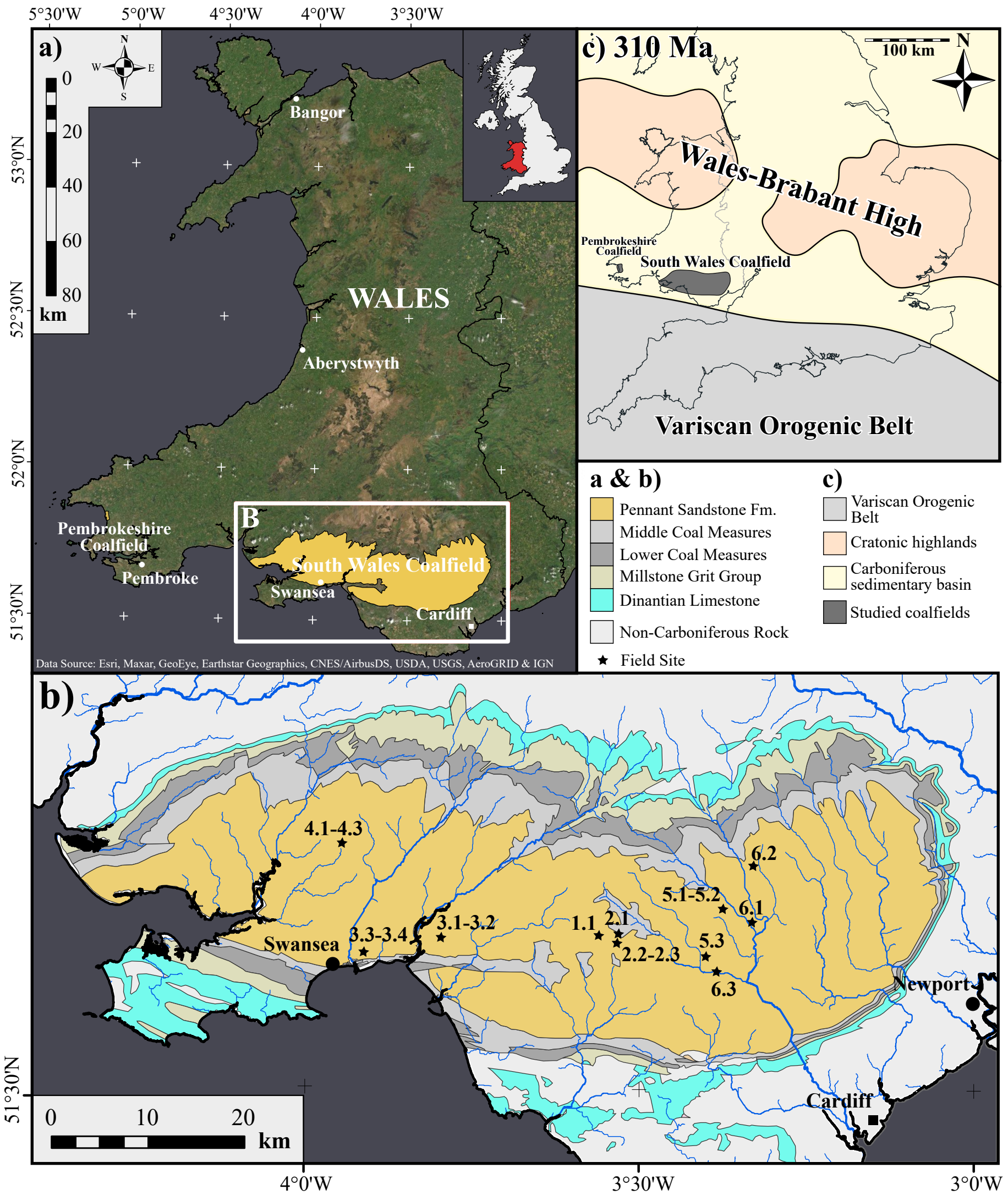
924 Fig. 8 - Trampush et al. (2014) palaeoslope boxplots for each locality arranged by longitude showing
925 possible downstream trend in palaeoslope. Pemb. = Pembrokeshire Coalfield. Legend as Fig. 6. Note.
926 field sites in each member are not known to be of the same fluvial system. Swansea member is not
927 included here as field sites do not show sufficient spatial variation.

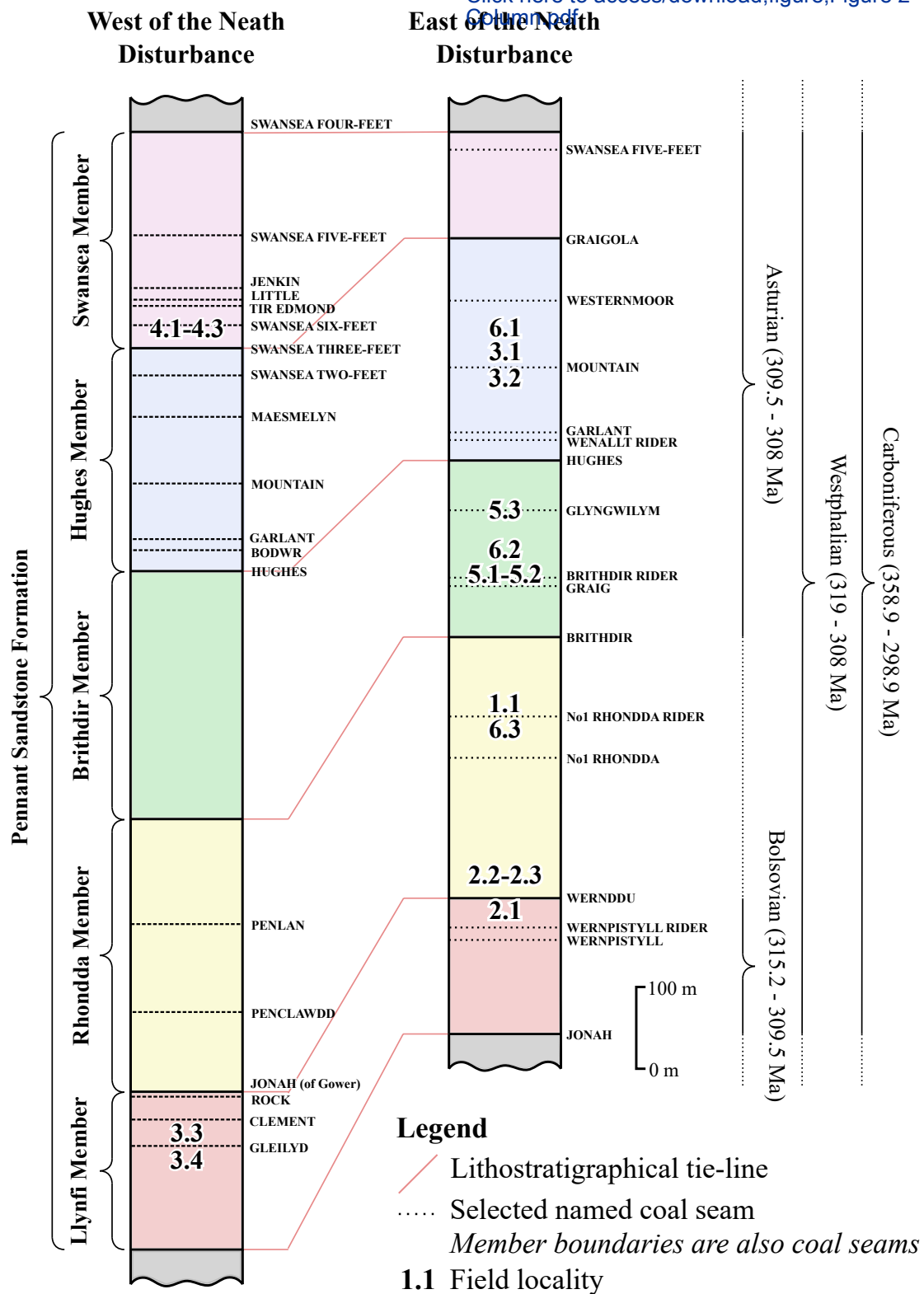
928 Fig. 9 - Summary of single-thread and channel belt widths and discharges in the Pennant Sandstone
929 Formation. **(a)** Widths calculated using the methods of Jones (1977; error = interquartile range),
930 Greenberg et al. (2021; error = standard error of Eq. 6), and the outcrop width. Arranged by locality,
931 west-east. **(b-d)** Cumulative frequency plots of water discharge assuming widths shown here and
932 unit discharges (Figure 6d) for each member. **(b)** Single-thread discharges using Greenberg et al.
933 (2021). **(c)** Channel belt discharge using outcrop width. **(d)** Channel belt discharge using Jones (1977)
934 width.

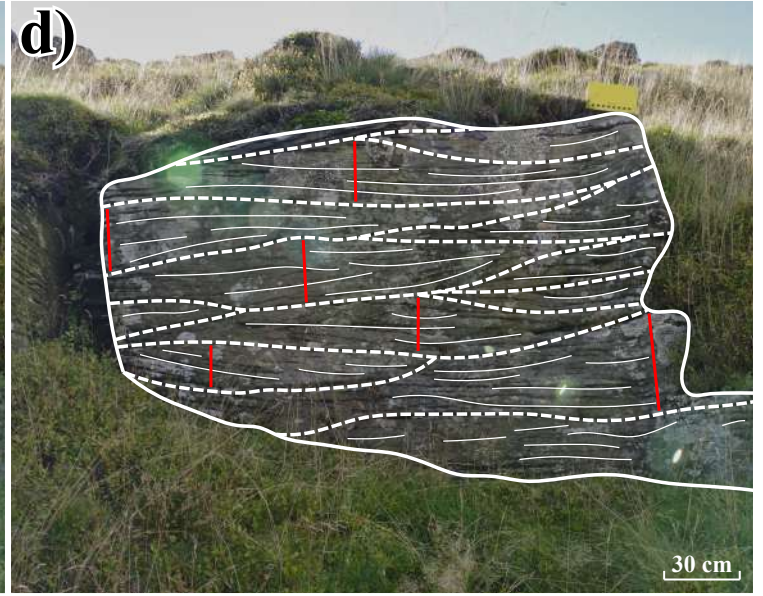
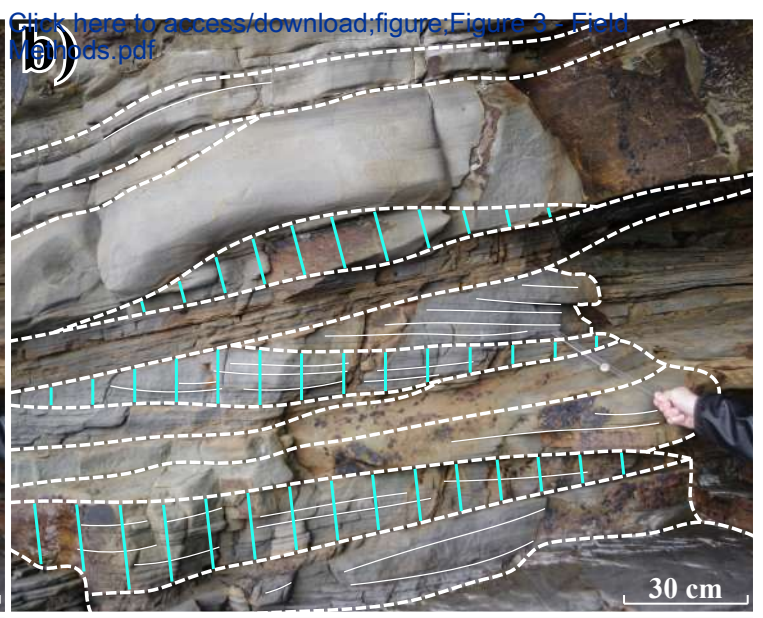
935 Fig. 10 - Plot predicting the fluvial style of the Pennant Sandstone Formation. Plot of H/W against
936 S/Fr using width estimates from Greenberg et al. (2021) and the outcrop width. Stability fields for
937 single- and multi-threaded systems of Parker (1976; grey dashed line) and Lyster et al. (2022;
938 red/green dashed lines) are shown.

939 Fig. 11 - Photographs of *Lepidodendron* wood preserved as clasts in conglomeratic horizons of the
940 Llynfi Member at Kilvey Hill, Swansea (Supplement 1). In places fossils exceed 1 m along their long
941 axis and are found in distinct sedimentary packages, in places forming clast-supported deposits of
942 wood clasts.

943 Fig. 12 - Graphical representation of the ancient rivers of the Pennant Sandstone. **(a)** Mean single-
944 thread channel cross section. **(b)** Average planform morphology. Note: single-threaded river sections
945 also exist but are not represented here. **(c)** Longitudinal cross-section showing mean flow depths,
946 dune heights and palaeoslopes. Note: slope is heavily exaggerated.



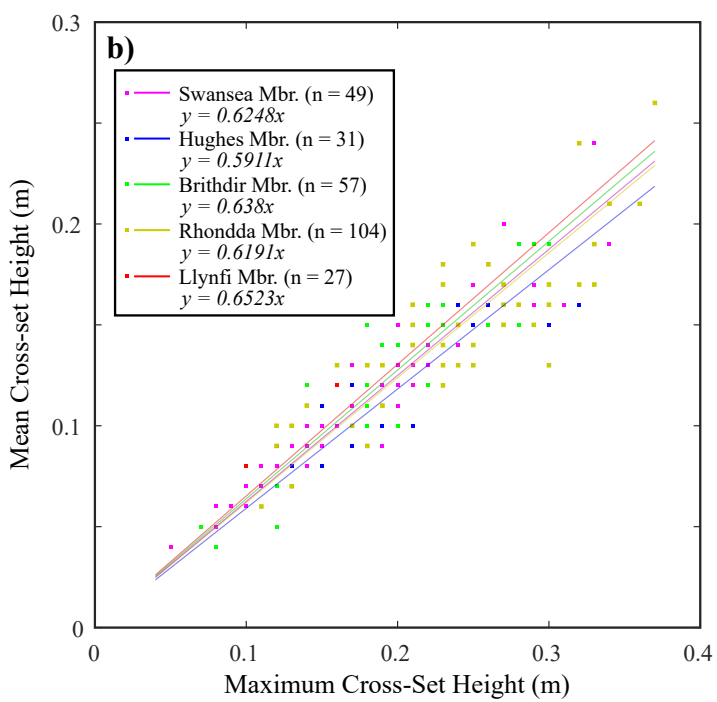
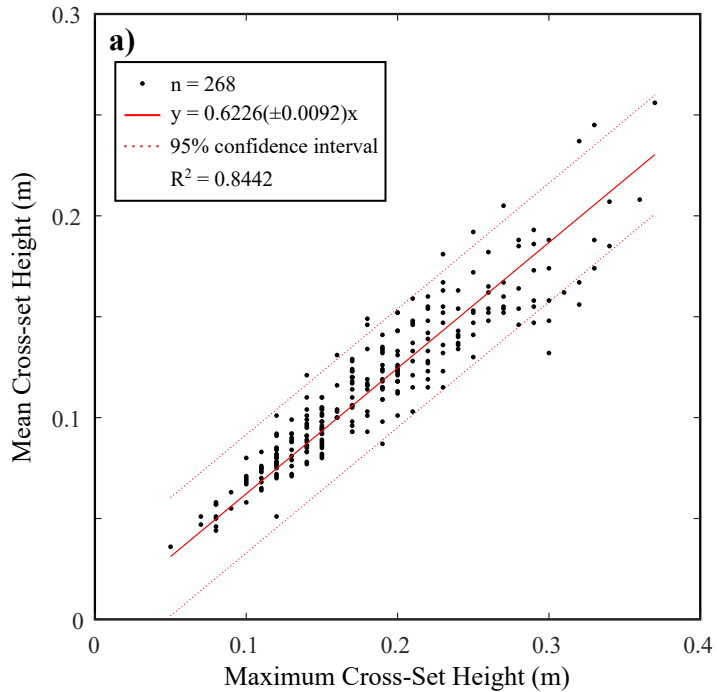


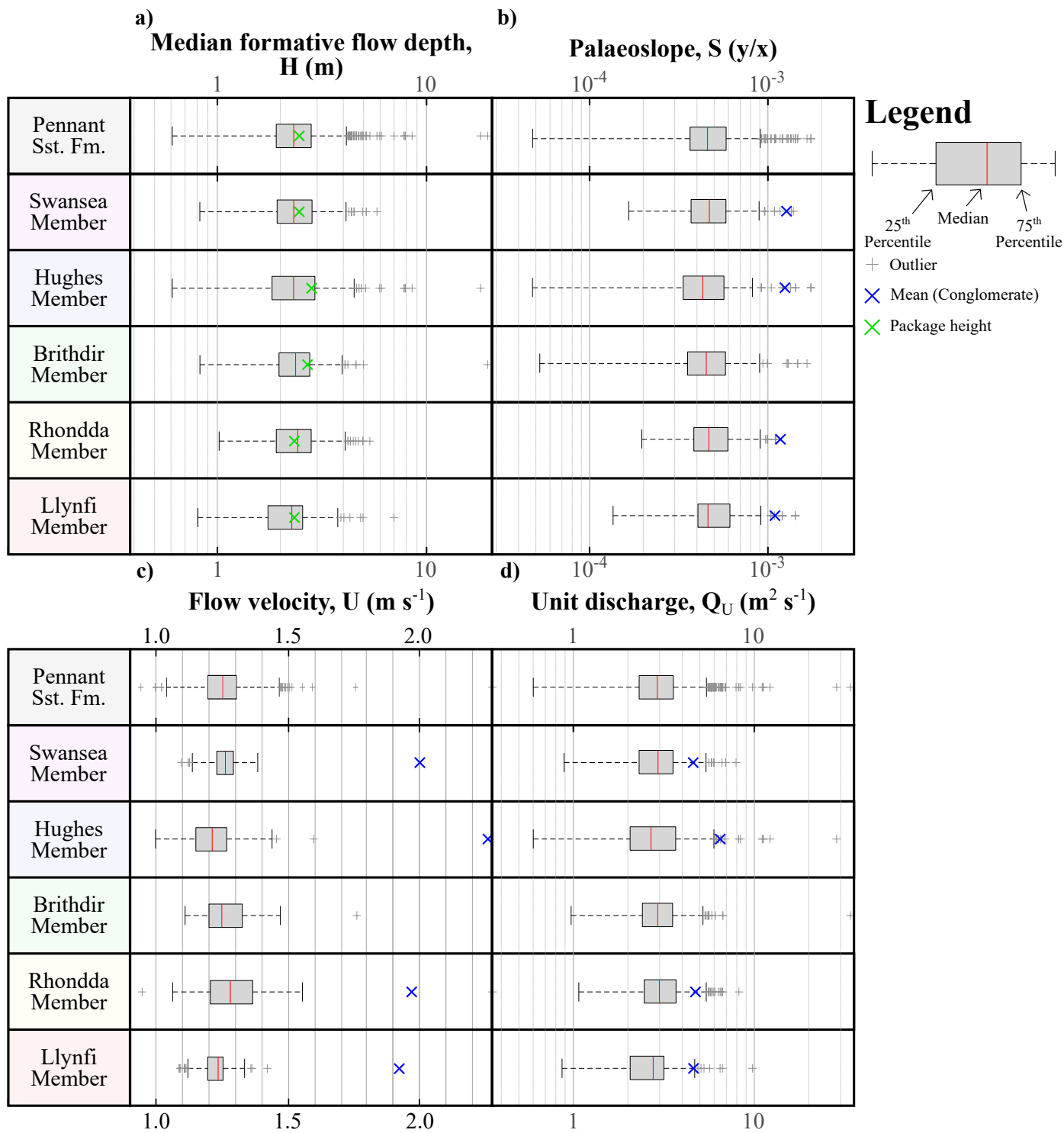




— Accretion/channel packages — Accretion/bedding surfaces — Vegetation

figure 5





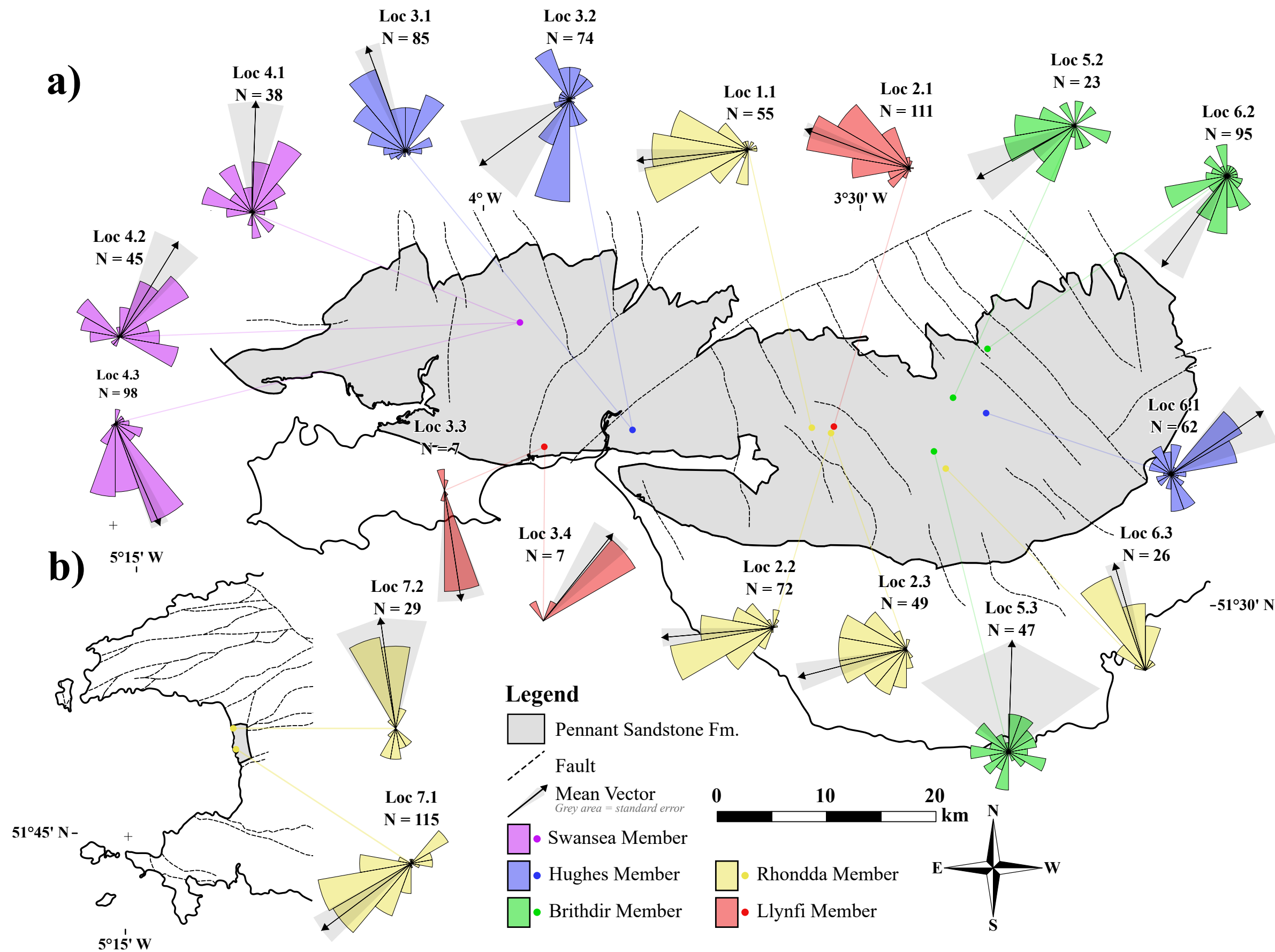


figure 8

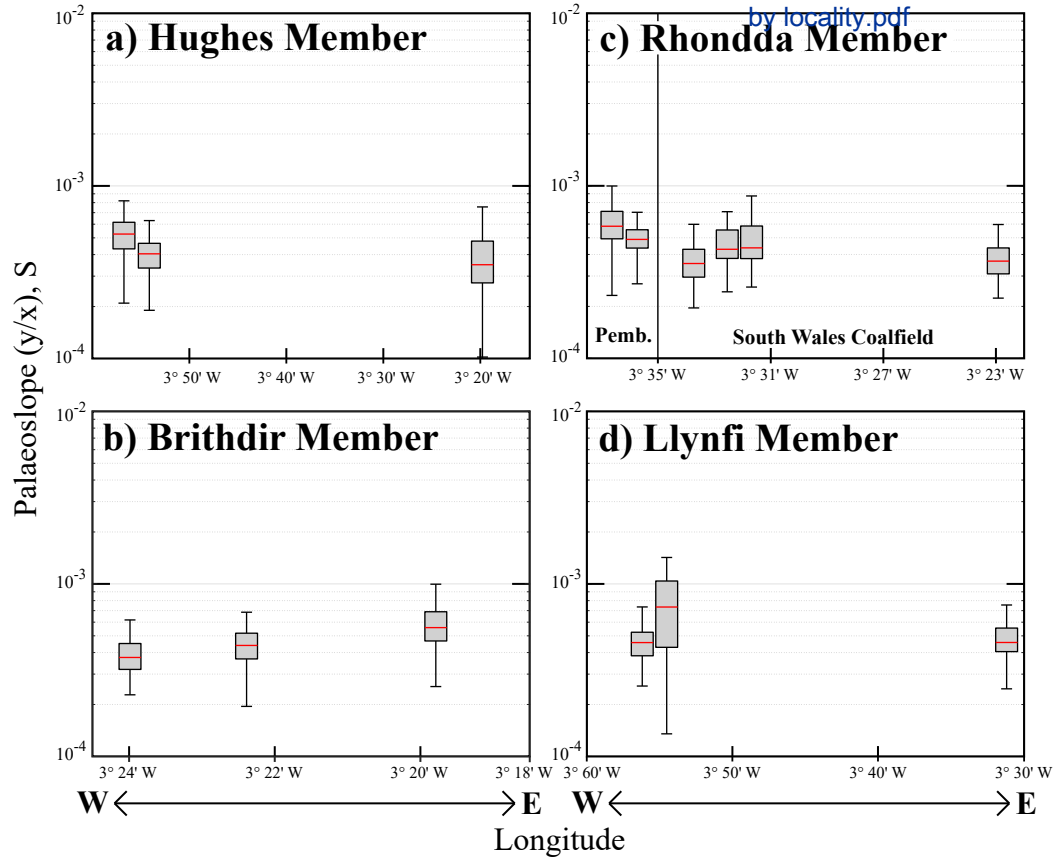
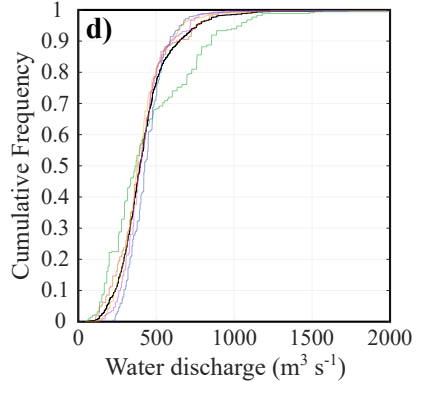
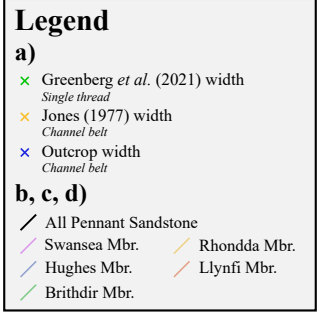
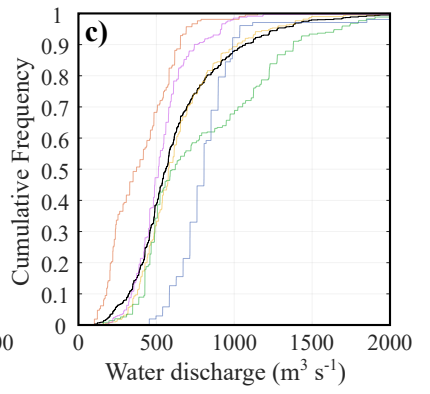
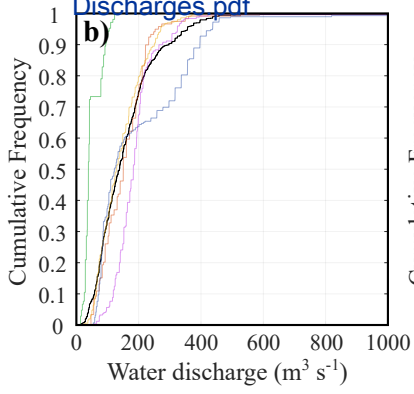
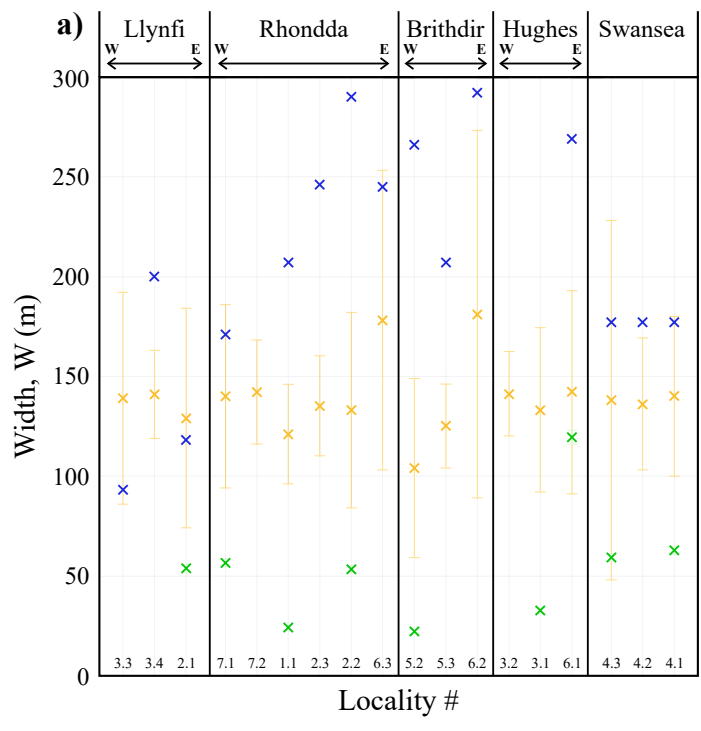
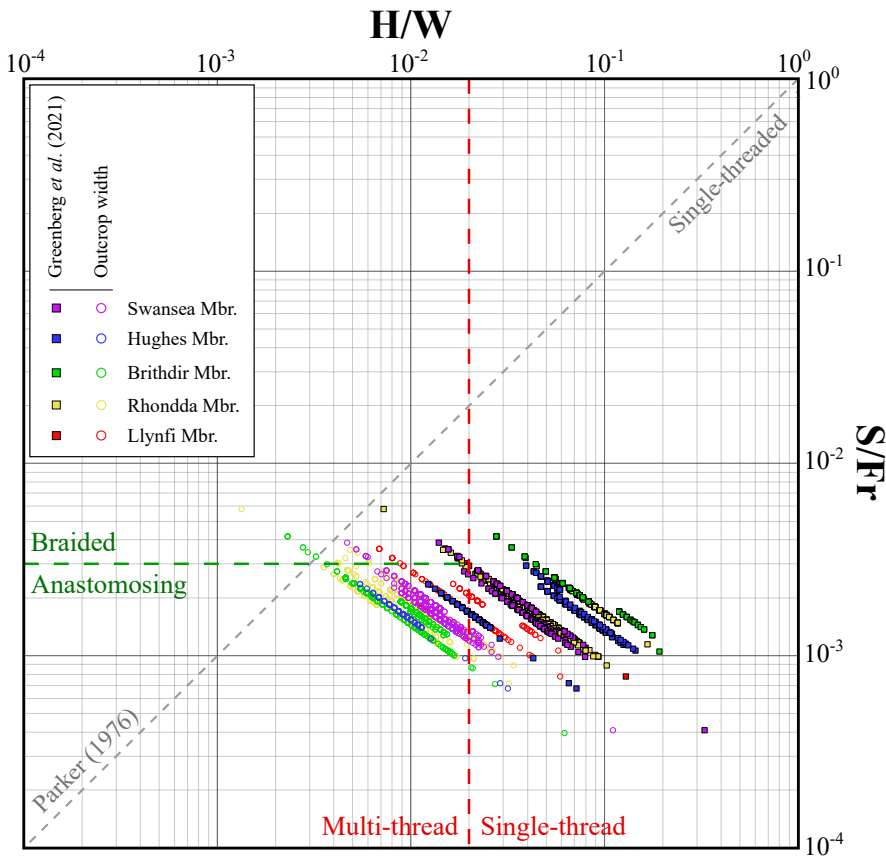


figure 9

[Click here to access/download;figure;Figure 9 - Widths and Discharges pdf](#)





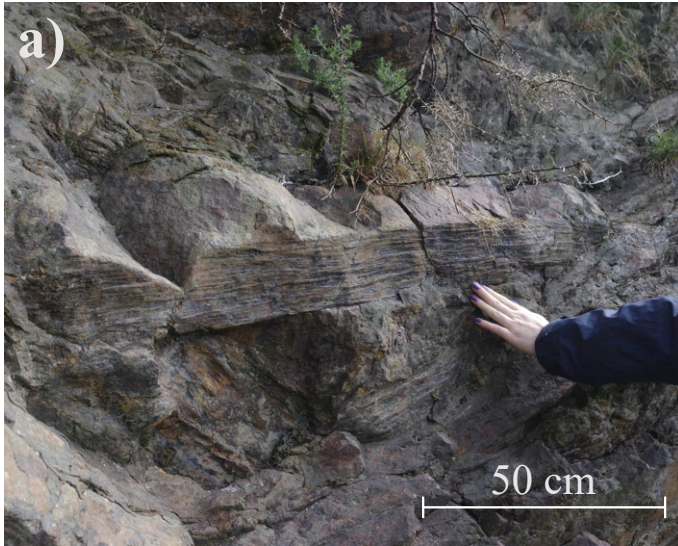
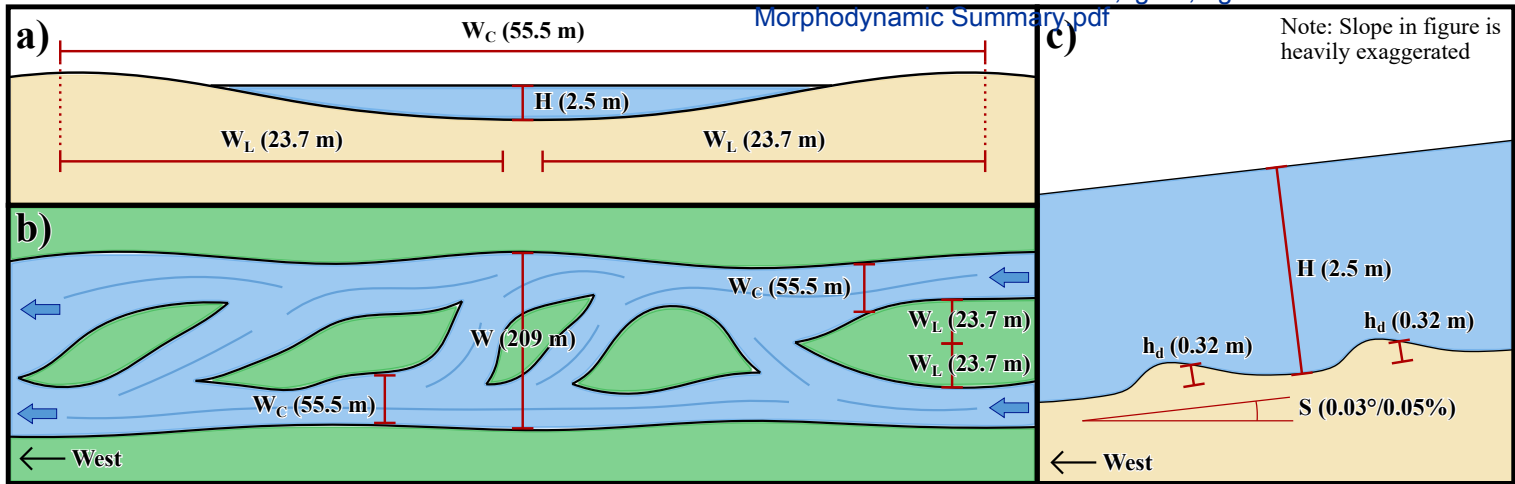


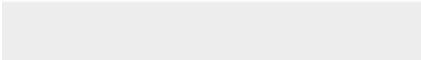
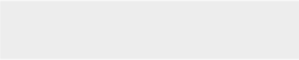
figure 12





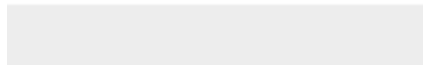
Click here to access/download
supplementary material

Rivers of the Variscan Foreland - Supplementary
Information.docx



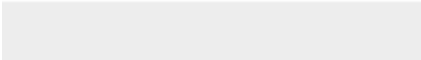
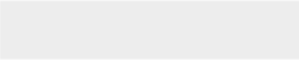


Click here to access/download
supplementary material
Field Data.xlsx



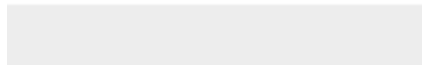
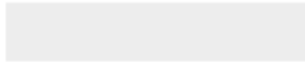


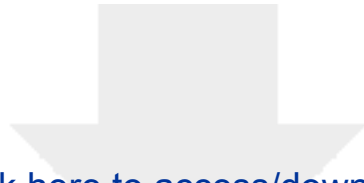
Click here to access/download
supplementary material
doc.kml





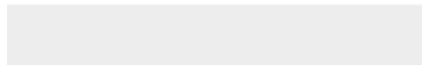
Click here to access/download
supplementary material
Figure S1 - Scaling Verification.pdf





Click here to access/download
supplementary material

Figure S2 - Facies Rose Diagrams.pdf





Click here to access/download
supplementary material
KS tests.xlsx

THE PROBLEM OF PALEO-PLANFORMS

Sinéad J. Lyster¹, Alexander C. Whittaker¹ and Elizabeth A. Hajek²

¹*Department of Earth Science & Engineering, Imperial College London, UK.*

²*Department of Geosciences, The Pennsylvania State University, USA.*

**s.lyster17@imperial.ac.uk*

Manuscript received: 15 November 2021

Revised manuscript received: 5 February 2022

Manuscript accepted: 9 February 2022

DOI: 10.1130/G49867.1

ABSTRACT

Reconstructing river planform is crucial to understanding ancient fluvial systems on Earth and other planets. Paleo-planform is typically interpreted from qualitative facies interpretations of fluvial strata, but these can be inconsistent with quantitative approaches. We tested three well-known hydraulic planform predictors in Cretaceous fluvial strata (in Utah, USA) where there is a facies-derived consensus on paleo-planform. However, the results of each predictor are inconsistent with facies interpretations and with each other. We found that one of these predictors is analytically best suited for geologic application but favors single-thread planforms. Given that this predictor was originally tested using just 53 data points from natural rivers, we compiled a new data set of hydraulic geometries in natural rivers ($n = 1688$), which spanned >550 globally widespread, sand- and gravel-bed rivers from various climate and vegetative regimes. We found that the existing criteria misclassified 65% of multithread rivers in our data set, but modification resulted in a useful predictor. We show that depth/width (H/W) ratio alone is sufficient to discriminate single-thread ($H/W > 0.02$) and multithread ($H/W < 0.02$) rivers, suggesting bank cohesion may be a critical determinant of planform. Further, we show that the slope/Froude (S/Fr) ratio is useful to discriminate process in multithread rivers; i.e., whether generation of new threads is an avulsion-dominated (anastomosing) or bifurcation-dominated (braided) process. Multithread rivers are likely to be anastomosing when $S/Fr < 0.003$ (shallower slopes) and braided when $S/Fr > 0.003$ (steeper slopes). Our criteria successfully discriminate planform in modern rivers and our geologic examples, and they offer an effective approach to predict planform in the geologic past on Earth and on other planets.